A new HW Vir binary from the MUCHFUSS project

A quantitative analysis of optical spectra and lightcurves

Bachelorarbeit aus der Physik

vorgelegt von

Ingrid Barbu-Barna

Bamberg, 14. August 2013

Dr. Karl Remeis Sternwarte Bamberg
Astronomisches Institut der
Friedrich-Alexander-Universität Erlangen-Nürnberg

Friedrich-Alexander-Universität Erlangen-Nürnberg

ecap ERLANGEN CENTRE FOR ASTROPARTICLE PHYSICS

Betreuer: Prof. Dr. Ulrich Heber

Contents

List of Figures

List of Tables

Abstract

We report the discovery of an eclipsing binary system - SDSS 192059+372220.0 - being a subdwarf B star with a faint companion. This binary was found in the MUCHFUSS project - Massive Unseen Companions to Hot Faint Underluminous Stars from the Sloan Digital Sky Survey (SDSS) - and belongs to the group of rare variable stars which are named after the prototype HW Vir. With this system the thirteenth of such HW Vir systems is found. The lightcurve shows grazing eclipses and a strong reflection effect.

This thesis deals with the analysis of time-series spectroscopy and photometry of SDSS 192059+372220.0 obtained at 2-4 m class telescopes (DSAZ, Calar Alto and ING, La Palma). An orbital period of 0.168830 days, an inclination of $i = 65.541°$, a mass ratio of $q = 0.24$, a radial velocity semiamplitude $K_1 = 57.20 \pm 2.44$ kms^{-1} and system velocity of $\gamma = 17.9 \pm 1.78$ kms^{-1} were determined from a combined spectroscopic and photometric analysis, as well as surface parameters. The atmospheric parameters ($T_{\mathrm{eff}} = 27600$ K, $\log g = 5.40$ and $\log n_{\mathrm{He}}/n_{\mathrm{H}} = -2.50$) are consistent with a core helium-burning star located on the extreme horizontal branch, being therefore a subdwarf B primary. The mass was derived, thus, to be $M_{\mathrm{sdB}} = 0.483 M_\odot$. With a mass of $M_{\mathrm{comp}} = 0.115 M_\odot$ and a radius of $R_{\mathrm{comp}} = 0.216 R_\odot$ the companion is a late M-dwarf. Since the period is short, the system must have gone through a common envelope phase.

1 Introduction

After some centuries of observation two categories of stars are known: the single ones, like the Sun, and the binary or multiple systems, like for example Sirius A and B or Castor. Beginning with the invention of the telescope around 1610 some stars on the sky were resolved into a pair of stars like for example Sagitarii. But at that time, there was no evidence, that all the observed pairs of stars on the sky are physically linked; they are called double stars. Nevertheless, Michell commented 1767 that there might be a physical interaction between these stars. Friedrich Wilhelm Herschel supported this assumption with results of 40 years of observation. His sister Caroline and his brother Alexander helped him to determine the relative motions on the sky of the observed pair of stars are due to orbital motion in accordance to Newton's law. Hence, there was now a new nomenclature to distinguish between the optical *double stars* - they are only by chance pairs that are really at very different distances from us - and the *binary stars* - they are physically linked by gravitational force.

During the nineteenth century other investigations of binary systems were made, notably by J. South, J. Herschel, F. Bessel, F.G.W. Struve, O. Struve and S.W. Burnham. The last one mentioned published the "*Catalogue of Double Stars within* $121°$ *of the North Pole*" in 1906 with information of 13665 binary systems.

In 1670, β Persei was discovered and called "the Demon" due to unexplainable brightness variations. But

Friedrich Wilhelm Herschel[1]

1783 these variations were explained by John Goodricke as eclipses. In this case, a *close binary star* which is not resolvable, was detected and β Persei was shown to actually be a binary system.

With the development of spectroscopy (around 1889), even the orbital variation is observed in the spectral lines of stars: they can be either single or double-lined.

Until today further data for binaries are collected: the orbits of visual ones, the velocities of spectroscopic ones and the flux variations of eclipsing ones. It is still an aim of research to determine the mass of the binary stars or to understand the formation of binaries or multi-star systems (Hilditch 2001).

This senior thesis will deal with close binary systems, especially of close binaries with a subdwarf B as primary. Subdwarf B stars with their characteristics and their importance will be mentioned, as well as HW Virginis systems.

The thesis is organised as follows: in chapter two the spectra of stars and the known spectral classes are explained. Afterwards, the most important cases of stellar evolution for this thesis will be presented. Binary systems and subdwarf B stars will be introduced in the following chapter. The methods of analysis and the results of the analysed HW Virginis system SDSS 192059+372220.0 are explained and presented in the last chapter.

---

[1]Figure taken from `http://www.dsi.uni-stuttgart.de/bildungsprogramm/lehrmaterial/ir-strahlung/pics/herschel.gif`
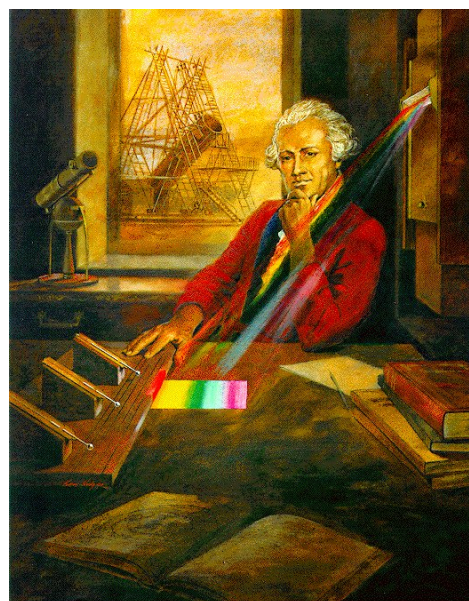
2 Spectrum and spectral classes

The information of the following chapters 2 to 4 is taken from Karttunen et al. (2007).
All information about stars is obtained from observations and analysis of their spectra. The spectrum of a star is a continuous spectrum with narrow spectral lines, mostly absorption lines but sometimes also emission lines. First, it was Joseph Fraunhofer who observed 1814 these dark lines in the spectrum of our Sun. Hermann Carl Vogel, a german astronomer, analysed stars, planets, comets and the Sun spectroscopically and attempted spectral classifications first. Angelo Secchi, an italian pioneer of the astrophysics, examined over 4000 stellar spectra and was the first to create the spectral classifications, and William Huggins developed a powerful spectrographic telescope apparatus and determined essential compositions of stars and nebulae. At that date, stellar spectroscopy, like it is known today, began.[2]
The strength of a certain absorption line corresponds to the number of atoms in the atmosphere that are in the same state to absorb photons at the apropriate frequency.
Such spectral lines can reveal surface temperature and gravity or even chemical composition of the atmosphere of the observed star.

2.1 Balmer lines

In 1859, G. Kirchhoff and R. Bunsen showed that atoms are only able to absorb or emit the light of certain wavelengths. These absorption or emission spectra are characteristic for every atom. In 1885, J.J. Balmer was able to describe the emission spectrum of the hydrogen atom by using a simple equation, since he noticed that a spectrum is a serie of lines. Just five years later this equation was generalized by J. Rydberg to:

$$\nu = R_{\mathrm{H}} c \left(\frac{1}{m^2} - \frac{1}{n^2} \right) \qquad (2.1)$$

where ν is the frequency, c the speed of light, $n, m \in \mathbb{N}, n \geq m+1$ and R_{H} is the Rydberg constant, $R_{\mathrm{H}} = 1.09 \cdot 10^7 m^{-1}$. Here, n and m are the main quantum numbers, while m describes the ground state and n the excited state. Equation 2.1 can be transformed for the wavelengths and results in:

$$\frac{1}{\lambda} = R_{\mathrm{H}} \left(\frac{1}{m^2} - \frac{1}{n^2} \right). \qquad (2.2)$$

Figure 2.1: The different series of lines in a spectrum. Next to the arrows, the wavelength given in nm are noted. [3]

These lines are well known from the visible spectral range of wavelengths of 3600 to 8000 Å. They are known as $H_\alpha, H_\beta, H_\gamma, H_\delta$ and so

---

[2]Information taken from http://www.library.ethz.ch/exhibit/sonne/biogrSecchi07.html, http://www.uh.edu/engines/epi1845.htm and http://phys-astro.sonoma.edu/BruceMedalists/Vogel/
[3]Figure taken from http://library.thinkquest.org/C006669/media/Chem/img/Series.gif

on. Besides, other series are known aswell, like the Lyman series in the UV or the Paschen lines in the infrared. All these lines are shown in figure 2.1.[4]

2.2 The Harvard Spectral Classification

The spectra of stars can be divided into several classes. The most common classification scheme is known as the Harvard Spectral Classification since it was developed at the Harvard Observatory in the United States by some women, for example Annie Jump Cannon and Cecilia Payne-Gaposchkin. Cannon arranged the stars by their temperature, while Payne-Gaposchkin extended this classification project and realized that the spectral variations among stars were mostly a reflection of temperature. These two women were the first women to work at Universities in physics and research.[5]

  The Harvard Spectral Classification is based on the presence and strengths of absorption lines of various atoms and ions. Therefore, it is known as the following sequence:

$$\begin{array}{ccccccccc} & & & & & & C & & \\ O & B & A & F & G & K & M & L & T \\ & & & & & & S & & \end{array}$$

All these classes are divided in subclasses from 0 to 9 with decreasing temperature. Additionally, for every temperature different lines and bands are visible. In the following, the different classifications are presented briefly:

O: These stars are blue with temperatures of 30000 K to 50000 K. Mostly, He II, C III, N III, O III or Si IV lines are the strongest ones. Besides He II lines are visible, but H I lines are relatively weak.

B: They are blue-white stars with a surface temperature from 10000 K to 30000K. No He II lines are visible, He I lines are strong at the beginning, but for B9 stars they have disappeared. Hydrogen lines (H I) increase in strength.

A: White stars with surface temperatures of about 9000 K and very strong hydrogen lines getting weaker to later spectral subtypes, are of this type. Ca II lines are getting stronger and He I lines are not visible. Neutral metal lines appear.

F: They are yellow-white stars and have surface temperatures of about 7000 K with hydrogen lines getting weaker and Ca II getting stronger. Metal lines like Fe I and Fe II or Cr II are clearly visible.

G: Sun-like yellow stars appear with temperatures of about 5500 K. The H I lines still get weaker and Ca II lines are the strongest ones at G0. Atomic metal lines are getting stronger.

K: Stars with an orange-yellow color and temperatures of about 4000 K are of this type. The spectrum of such a star is dominated by metal lines. TiO bands are for the first time visible.

---

[4]Information taken from http://www.ipc.uni-stuttgart.de/demokurs/Balmer-Serie.pdf and http://www.chemie.de/lexikon/Balmer-Serie.html

[5]Information taken from http://m.teachastronomy.com/astropedia/article/Spectral-Classification

M: These stars are red ones with surface temperatures of about 3000 K. The TiO bands are getting stronger.

L: That is the class of very red stars with a surface temperature of about 2000 K. The TiO bands disappear and Na I and K I become visible and broad.

T: These stars are extremely red and emit light mostly in the infra red. They have temperatures of about 1000 K. Here, strong molecular absorption bands of CH_4 and H_2O show up, similar to the spectra of Jupiter.

C: These stars are a subclass of the red stars, termed carbon stars, because strong atomic and molecular carbon lines are visible. They have similar surface temperatures as M stars but no TiO band exists.

S: Another subclass of red stars with lower temperatures (nevertheless about 3000 K) characterizes this type. Other molecular bands are visible such as YO or TiO.

These characteristics are summerized and shown in figure 2.2.
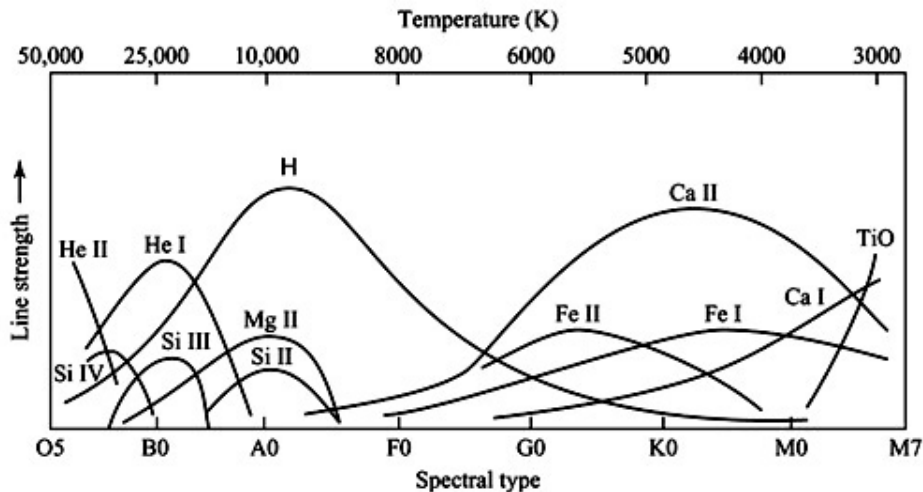
Figure 2.2: The main characteristics of the Harvard Spectral Classification are presented. The variations of lines for the different spectral classes are shown clearly.[6]

2.3 The Yerkes Spectral Classification

A two dimensional spectral classification scheme is the Yerkes Spectral Classification which builds upon the Harvard system but adds the luminosity as a second parameter. There are six classes:

  Ia the most luminous supergiants,
  Ib the less luminous supergiants,
  II the luminous giants,
  III the normal giants,

IV the subgiants,

V the main sequence stars (dwarfs),

VI the subdwarfs.

These classes are determined from the shape of the spectral lines which are sensitive to density. For a given mass the atmospheric density depends on the size of the stars. So does the gravitation. With increasing radius R of a star the gravitational acceleration g and the atmospheric density ρ decrease

$$g = \frac{GM}{R^2} \text{ and } \rho = \frac{M}{V} \tag{2.3}$$

where G is the gravitational constant and M the mass of the star. Therefore, the gas density and pressure in the giants' atmosphere is much smaller which reduces the line broadening due to the Stark-effect and gives rise to lines more narrow than in the higher density of dwarf stars. Additionally, with increasing radius the luminosity increases as well

$$L = \sigma A T_{\text{eff}}^4 = \sigma 4\pi R^2 T_{\text{eff}}^4 \tag{2.4}$$

with $\sigma = 5.6705 \cdot 10^{-8} W m^{-2} K^{-4}$ the Stefan-Boltzmann constant and T_{eff}^4 the effective temperature of the star. That is the reason why the Yerkes Spectral Classification can also be used as a luminosity indicator.

Unfortunately, subdwarf O and B stars can not be classified in the classical scheme.

2.4 The Hertzsprung-Russell Diagram
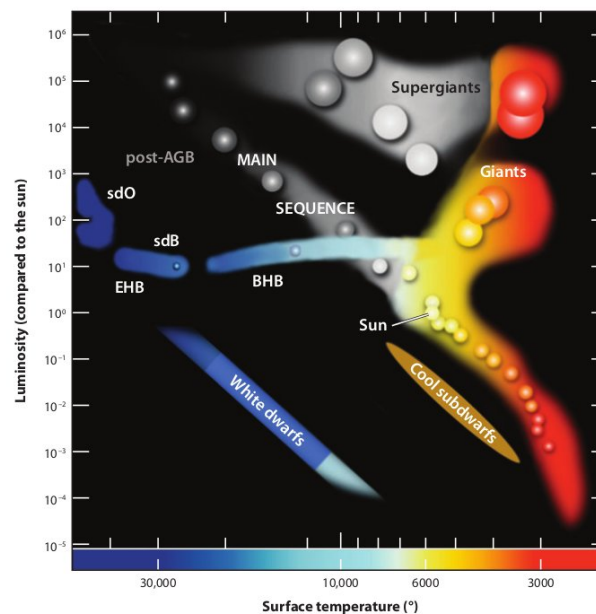
Figure 2.3: The Hertzsprung-Russell diagram. On the x-axis the surface temperature is noted, on the y-axis the luminosity compared to the sun. This diagram is taken from Heber, 2009 review.

In 1910, E. Hertzsprung and H.N. Russell studied the relation between the absolute magnitude and the spectral types of stars. These studies were linked in a diagram, the *Hertzsprung-Russell Diagram*, an important instrument for astronomy. In figure 2.3 the phases of stellar evolution and some characteristics, like temperature and luminosity, are shown. Right in the middle of the diagram, the long diagonal line, is the *main sequence*. Depending on the mass of the stars they are located either on the left top (with masses greater than $1 M_\odot$) of this main sequence - towards larger sizes and higher luminosities - or on the right bottom (with masses smaller than $1 M_\odot$). Being on the main sequence the star is in a stable evolution stadium (see section 3.1).

Right under the main sequence the *cool subdwarfs* are located, begin part of the main sequence of the old metal-poor population.

On the left side of the cool subdwarfs the *white dwarfs* are shown. With their small radii and their relatively high masses, they are less luminous than the main sequence stars despite their high central temperatures. They represent the terminal stage of a star main sequence star with masses comparable to the Sun.

Above the main sequence the giants are located, divided in red giants and supergiants. They have large radii and, thus, high luminosities.

For this senior thesis the blue horizontal branch (EHB), located right in the middle of figure 2.3 is important. There, the hot subdwarfs, like the sdB's and the sdO's are located. Their exact locations and their characteristics are explained further in chapter 5.

3 Stellar Evolution

In this chapter the stellar evolution is explained briefly, beginning directly with the main sequence phase. How a star is formed is not relevant to understand the further chapters, so it will not be explained.

3.1 The Main Sequence phase

On the main sequence the star spends the longest part of its life. The star releases all of its nuclear energy by hydrogen burning in the core which is the only source of energy of this star. It is in a stable equilibrium and its chemical composition changes only due to the nuclear reactions in its core.

More massive stars do not rest that long on the main sequence than less massive stars because they radiate more energy per mass what makes them leave these sequence earlier.

There is an upper mass limit for stars to form due to radiation pressure. It lies between $120M_\odot$ and $150M_\odot$. A lower-mass limit exists, too. An object with a mass less than $0.08M_\odot$ never becomes hot enough to begin hydrogen burning. They are called *brown dwarfs* and have surface temperatures of about 1000 K to 2000 K (see section 2.2). Many of the L and T dwarfs are likely brown dwarfs.

The evolution of low mass stars between $0.08M_\odot$ and $0.26M_\odot$ is simple: during the whole main sequence phase they remain fully convective and they will use all of their hydrogen to burn. After having it burned completely to helium, they contract to become white dwarfs.

3.2 The Giant phase

More massive stars do not burn their mass completely. When the hydrogen is ran out in the center it is burned in a shell surrounding an inert helium core. The mass of the core increases which leads to an expansion of the hydrogen envelope: the star becomes a giant closing up to the Hayashi track, that is where the star becomes almost fully convective. Because the star cannot cool down any more, its luminosity increases: the star becomes a red giant.

Stars with masses exceeding $2.3M_\odot$ do not have a core with degenerated electron gas, so the helium burning can set in while the central regions are contracting. When helium burning is now ran out it will continue to burn in a shell. Depending on the mass of the star, this mechanism of burning element and afterwards continuing burning in a shell can repeat until silicon - for stars with masses greater than $8M_\odot$ - is burned in the core. Silicon will continue burning in a shell, while the core consists of iron. This is the last stage of core burning. When this burning is ending the central pressure will decrease and the core collapses. All the other elements are burned in the shell, like a layer. The implosion of the core will result in the formation of a neutron star or a black hole.

If the star has just a mass less than $2.3M_\odot$ (but more than $0.26M_\odot$) the core mass grows and the electron gas becomes degenerated. Therefore, the temperature in the center rises and the whole helium core has an uniform temperature since the degenerated gas has a high conductivity. When the core reaches a temperature of more than 100 million degrees helium burning is set in in the central region and the temperature rises, but due to the degenerated gas the star cannot expand leading to an increasing energy production. After some time with rising temperature, the core will violently begin to expand, when the degeneracy of the electron gas is lifted. Just a few seconds afters the helium ignition, there is an explosion, known as *helium*

flash. Luckily this does not lead to a disruption of the star. After this flash the star begins a new state and helium is steadily burning to carbon. This phase is called the Horizontal Branch and is of special importance for this investigation because hot subdwarf stars are closely related to the Horizontal Branch. When the helium supply in the core vanishes, another phase of evolution follows. The star possesses two shells in which hydrogen and helium are burned, respectively. The star evolves to giant dimensions again, climbing the asymptotic giant branch. Before carbon can be ignited, the star will expell its envelope and evolve into a stellar corpse, called white dwarf, when all nuclear fuel in the shell has been consumed.

4 Binary Systems

Stars can evolve quite differently when they are in binary or multiple systems. The reader should distinguish between *optical double stars* and *gravitational bound binaries*.

The optical double stars appear on the sky to be very close, thus, someone would say that must be a binary. But they are not gravitationally bound and their separation is so wide that they do not affect each other.

Contrary to the optical double stars, the gravitationally bound binaries are real binaries. They can be classed in four types of binaries:

1. Visual binaries

2. Astrometric binaries

3. Spectroscopic binaries

4. Photometric binaries.

Before explaining the different types of binaries, there will we a brief introduction to close binary systems, as it is important for further explinations.

4.1 Close binary systems

Binary systems were referred to be close binary systems when the components of those systems are so close together that the observer cannont visually resolve them spatially into two separate stars. Hence, these binaries are known to interact among each other or to exchange even mass (Hilditch 2001). They influence the star evolution mentioned in chapter 3.

Actually, the evolution of a single star is well defined by mass and radius of a star. In contrast, the evolution of close binary systems is not well understood. It it, for example, influenced by mass loss of the mass-exchanging stars in close binaries. The stars in such binaries become tidally locked and they can be distorted to the limits of their Roche lobes that are introduced by the Roche model (Hilditch 2001, p. 131).

4.1.1 The Roche Model

For close binary systems it is important to have a physical model that takes the ellipsoidal deformation due to tidal forces into account. The model is named after the astronomer Edouard Albert Roche who developed 1849 the Roche model. It is based on the three-body problem. A corotating coordinate system (see figure 4.1) is chosen that follows the rotation of the two stars about their center of mass. This model assumes both stars to be point masses M_1 and M_2 because the masses are concentrated in their centers. These two masses are separated by a distance a. The stars are located at distances r_1 and r_2, respectively, on the x-axis from the center of mass, placed at the origin. Thus,

$$r_1 + r_2 = a \text{ and } M_1 r_1 = M_2 r_2. \tag{4.1}$$

Including the centrifugal potential and dividing the effective potential energy by m, a small test mass located in the orbital plane (x-y) the effective gravitational potential Φ can be found:

$$\Phi = -G\frac{M_1}{s_1} - \frac{M_2}{s_2} - \frac{\omega^2}{2}r^2 \tag{4.2}$$
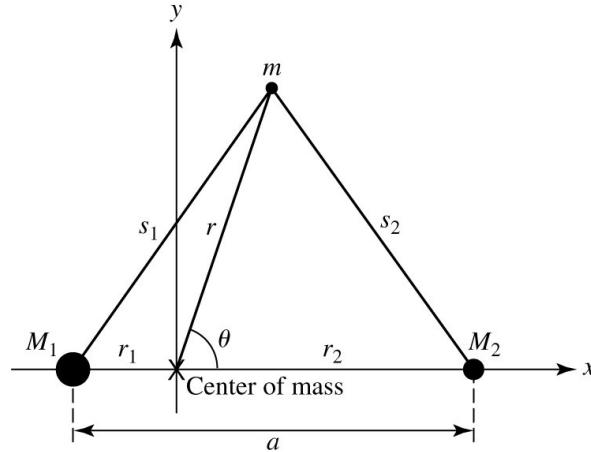
Figure 4.1: Co-rotating coordinates for a binary star system (Carroll & Ostlie 2007).

while $\omega^2 = \frac{G(M_1+M_2)}{a^3}$ is the constant angular velocity with a the distance to the origin, $r_1 = r_1^2 + r^2 + 2r_1r\cos\theta$ and $s_2^2 = r_2^2 + r^2 - 2r_2r\cos\theta$ (Carroll & Ostlie 2007).

In figure 4.2 the inner Lagrangian points, termed as L_1 to L_5, and the Roche equipotential surfaces can be calculated. At the Lagrangian points the gravitational forces of the binary become neutralized.

The Roche volume, also known as Roche lobe, is the maximum volume the star reaches before mass exchange begins, that means that every particle lying inside the Roche lobe is gravitationally bound to this lobe and every particle lying outside the Roche lobe of every star belongs gravitationally to the complete binary (Hilditch 2001).
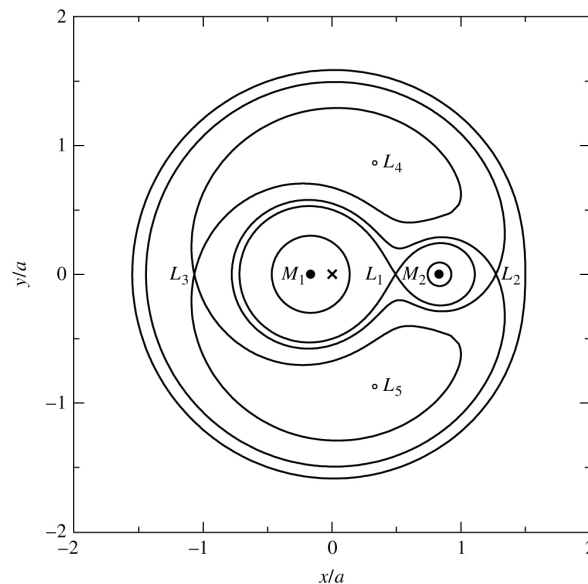
Figure 4.2: The equipotential surfaces known as Roche potential surfaces (Carroll & Ostlie 2007).

4.1.2 Types of close binaries

Three types of close binary stars exist: The *detached* binary system, the *semidetached* binary system and the *contact* binary system.

A detached binary is a system where every component with all its particles lies well defined inside its Roche-lobe which can be seen in figure 4.3(a).

When one of the components fills completely its Roche-lobe while the other one lies inside its Roche lobe volume, the binary is known as a semidetached one. This is demonstrated in figure 4.3(b).

If the components are in contact, both fill or even overfill their Roche-lobe. They form a common envelope, like shown in figure 4.3(c).
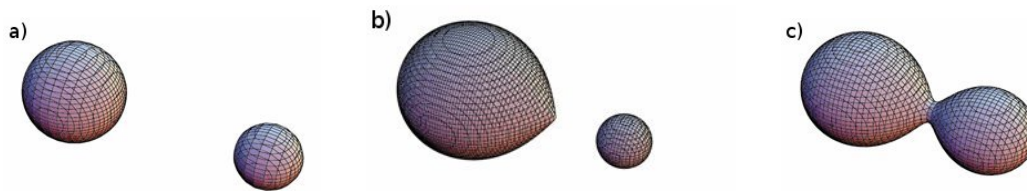
Figure 4.3: The different types of close binary systems: (a) A detached one, (b) a semidetached one and (c) a contact one.[7]

4.2 Visual binaries

The angular separation of the stars and the angular orientation of the secondary can be observed. Here, the brighter star is the primary which normally is considered to be fix and the fainter one is the secondary orbiting around the first one.

While the projection of the relative orbital ellipse on the plane of the sky can be measured by observations, the total mass can only be calculated, when the distance of the binary is known. With the help of Kepler's third law

$$\frac{P^2}{a^3} = \frac{4\pi^2}{G\left(m_1 + m_2\right)} \tag{4.3}$$

where m_1 is the mass of the primary and m_2 that of the secondary and P the period, and by observing the motion of both components relative to the center of mass, the semi-major axe a can be determined with

$$\frac{a_1}{a_2} = \frac{m_2}{m_1} \tag{4.4}$$

and

$$a = a_1 + a_2 \tag{4.5}$$

where a_1 is the semi-major axe of the primary and a_2 that of the secondary.

4.3 Astrometric binaries

In astrometric binaries only the motion of the brighter star about the center of mass is seen. Once the mass of the primary is estimated by analysing for example its luminosity, the mass

---

[7]Figure taken from http://astro.matf.bg.ac.rs/beta/lat/sci/CBS/Fig1.gif

of the companion can be estimated, too. The first discovered astrometric system was Sirius with its companion Sirius B as a white dwarf.

4.4 Spectroscopic binaries

The spectroscopic binaries seem to be single stars, but their spectra show a regular variation. The period of the variation is the orbital period of the stars. Additionally, the orbital period can be derived from the radial velocity which is related proportionally to the Doppler shift by

$$\frac{\lambda - \lambda_0}{\lambda_0} = \pm \frac{v_{\text{rad}}}{c} \tag{4.6}$$

where v_{rad} is the radial velocity, λ_0 is the laboratory wavelength of the spectral line and c the speed of light. The Doppler shift tells us if a star is moving away from (positive sign) or towards (negative sign) the observer as presented in figure 4.4.
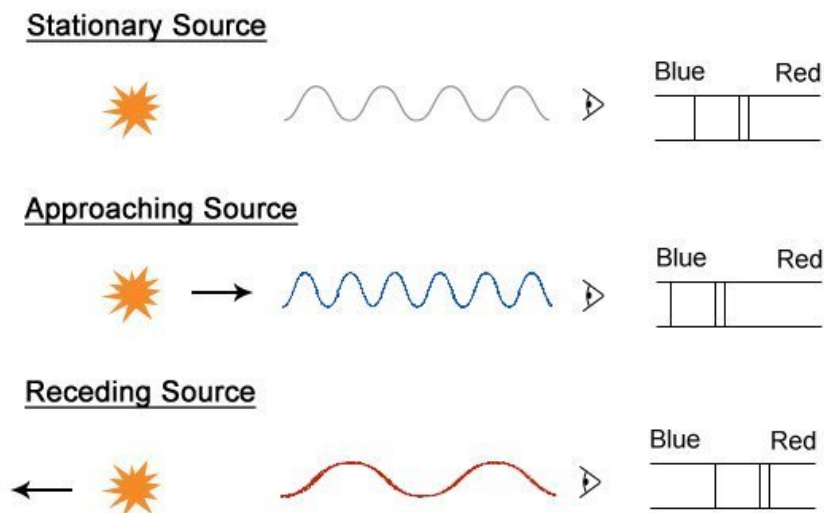
Figure 4.4: Demonstration of the Doppler-Shift. When the star is not moving the emitted wavelength is neither shortened nor lenghtened. If the star is approaching, the wavelength is shortened and the absorption lines are shifted to the blue range of the spectra. If the star moves away the emitted wavelength is lenghtened and the absorption lines shift to the red range of the spectra.[8]

4.4.1 Radial velocity curve

By using the Doppler shift as mentioned above the radial velocity curve can be obtained by fitting the radial velocity as a function of time. If this curve shows variations the presence of an invisible companion is proved.
The shape of the radial velocity curve tells us if the binary system orbits circularly, described

---

[8]Figure taken from http://lamost.us/legue/images/story_images/legue-science/doppler_shift_drop_shadow_redone.png

by a sinusoidal curve, or eccentrically. Most of the short period binaries have circular orbits. In figure 4.5 such a radial velocity curve is shown. This sinusodial radial velocity can be
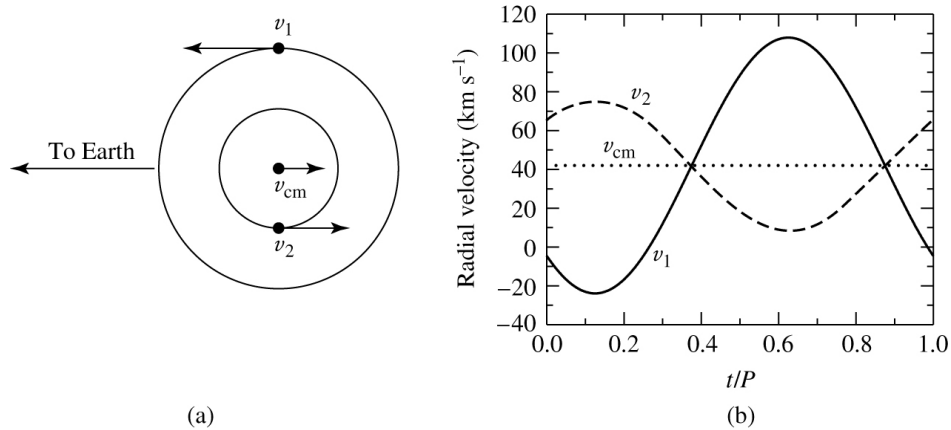
Figure 4.5: Two stars in circular orbits (a) and the resulting radial velocity curve (b) (Carroll & Ostlie 2007).

described by

$$v_{\mathrm{rad},1,2}(t) = K_{1,2} \sin\left(\frac{2\pi}{P}(t - T_0)\right) + \gamma \tag{4.7}$$

where γ is the velocity of the system, $K_{1,2} = v_{1,2}$ the semi-amplitude of the radial velocity, P the period and T_0 the time the companion is right in front of the primary. This velocity is just the apparent velocity. To get the real one v_0, the inclination i has to be known. Thus, we find the following equation:

$$v_0 = \frac{v_{\mathrm{rad}}}{\sin(i)}. \tag{4.8}$$

4.4.2 Single- and double-lined spectroscopic binaries

Two types of spectroscopic binaries exist, the *single-lined* spectroscopic binaries and the *double-lined* spectroscopic binaries.
If the companion has a mass larger than $0.45 M_{\odot}$ and if it is a main sequence star, too, this star influences the total visible spectrum of the binary system and the spectral lines double periodically, then merges into a large single line and, with the phase, redoubles again. Such double-lined spectra indicate the presence of two stars giving opposite Doppler shifts. In figure 4.6 double-lined spectral lines are displayed merging with the phase.

If the companion has only a mass smaller than $0.45 M_{\odot}$, or the spectral lines from the primary are stronger than those from the secondary, only a single-lined spectrum of the binary is visible. Nevertheless it is possible to figure out that the observed system is a spectroscopic binary because of the periodically shift of the radial velocity. But the masses cannot be determined exactly, there rests still a degeneracy of masses.[10]

---

[9]Figure taken from http://csep10.phys.utk.edu/astr162/lect/binaries/binspec.gif

[10]Information taken from http://csep10.phys.utk.edu/astr162/lect/binaries/spectroscopic.html
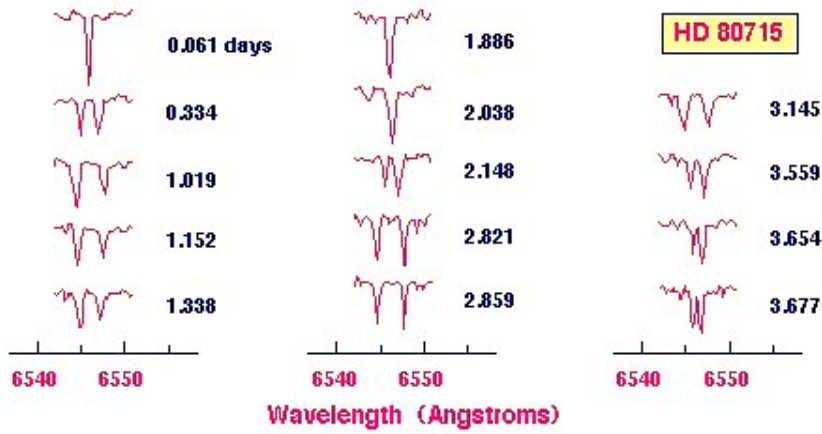
Figure 4.6: Double-lined spectra are displayed, mering with the phase.[9]

4.4.3 The mass function

For close binary systems (see section 4.1) the orbit is circularized by tidal forces. Thus, due to the theorem of center of mass

$$M_1 v_1 = M_2 v_2, \tag{4.9}$$

the mass ratio

$$q = \frac{M_2}{M_1} = \frac{a_1}{a_2} = \frac{K_1}{K_2} \tag{4.10}$$

and Kepler's third law (see equation 4.3), one can derive the mass function

$$f(M_1, M_2) = \frac{M_2^3 \sin^3(i)}{(M_1 + M_2)^2} = \frac{P K_1^3}{2\pi G} \tag{4.11}$$

with i the inclination of the system.

Knowing the mass ratio q (if the spectra of stars are single-lined), equation 4.11 can be transformed to

$$M_j \sin^3(i) = \frac{P}{2\pi G} \frac{K_j^3 (1+q)^2}{q^3} \tag{4.12}$$

and the separation a between both stars can be calculated by

$$a = \frac{P}{2\pi} \frac{K_1}{\sin(i)} \left(1 + \frac{1}{q}\right). \tag{4.13}$$

4.5 Photometric and eclipsing binaries

In photometric binaries a periodic variation in the brightness of the star is seen. Normally, they are known as eclipsing binaries, since the luminosity is diminished when the components are in front of each other. The deepness of the eclipses depends on the size of the stars as well as on the inclination angle i. Two types of eclipses exist, the *total eclipses* and the *partial eclipses*. If the binary is a total eclipsing binary, the secondary will not affect the surface parameters of the primary in half the phase, that is when the secondary is directly behind the primary. It will disappear completely. In a partial eclipsing binary the secondary can always be seen, even behind the primary. Thus, it affects the spectral lines of the primary and

makes the analysis more difficult. The best values for surface temperature, surface gravity and helium abundace can be determined only at phase zero, when the companion is in front of the primary and the contaminating light is minimal.

These periodic variation can be seen in the lightcurve, where the luminosity is shown as a function of time. There exist three subtypes of lightcurves.

4.5.1 Algol Stars - Detached Binaries

This type of stars is named after β Persei or Algol, an eclipsing variable star with a relatively constant brightness. The stars in this time of the lightcurve and period are seen separated from
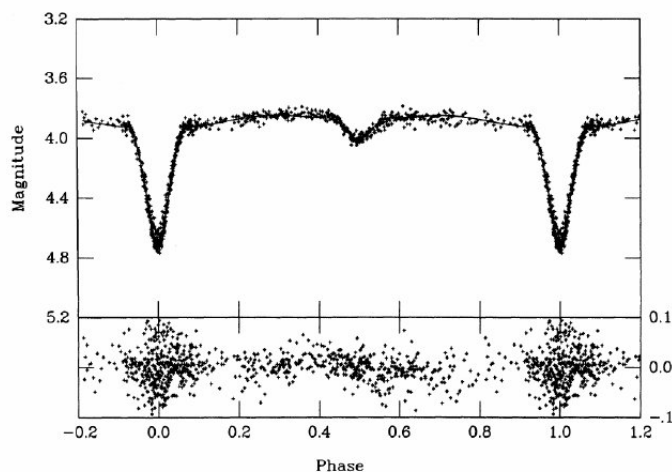
Figure 4.7: The lightcurve of a Algol-type star.[11]

each other, as well known as a detached system. In the lightcurve a small reflection effect is visible (for explanations of this effect see section 6.2). A similar effect that occurs every half period is the ellipsoidal effect due to tidal forces. There are two minima, too. The first one is usually deeper than the second one due to the brightness difference between both stars. When a larger, cooler star is passing the smaller and hotter one there is a deep minimum in the lightcurve visible, known as primary eclipse. If the smaller and hotter star is passing the larger and cooler one, there is a secondary eclipse that is not so deep as the first one, like the reader may notice in figure 4.7.

The form of the minima gives information about the inclination of the orbit and the duration gives information about the ratio of stellar radii.

---

[11]Figure taken from http://www.boulder.swri.edu/~terrell/talks/aavso2001/algol_ir.gif

4.5.2 β Lyrae Stars - Semi-detached Binaries

For this type of stars the luminosity changes constantly.   In this binary system one of the
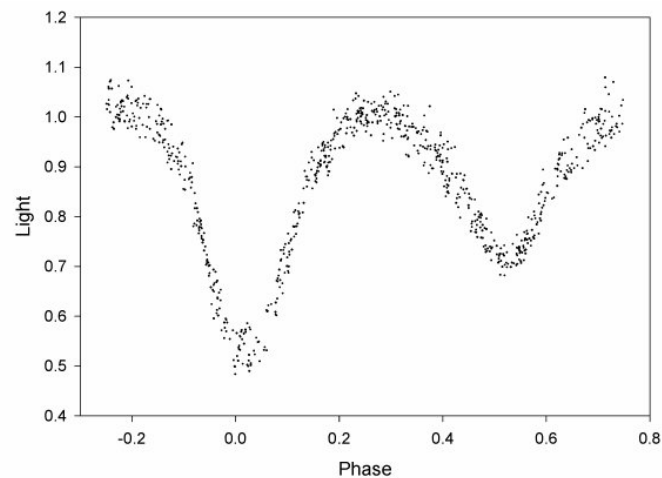
Figure 4.8: The lightcurve of a β Lyrae-type star. While the brightness of the star is changing
          constantly the binary is having a mass transfer due to the closeness of both
          components.[12]

stars has been pulled into an ellipsoidal form. Hence, the luminosity of the star changes also
outside the eclipses like it is shown in figure 4.8. These stars are so close that one of the
components has already filled its Roche lobe and a mass transfer takes place.

4.5.3 W UMa Stars - Contact Binaries

For this type of binary system - fig-
ure 4.9 - the lightcurve minima are
almost identical, very round and
broad. Here are, thus, very close
binary systems visible, where both
stars overfill their Roche lobe and
they form a contact binary sys-
tem. But W UMa stars cause diffi-
culties to interpret the lightcurve
due to several reasons. Being a
contact binary, the shape due to
tidal forces is distored or gravity
darkenig has to be considered.
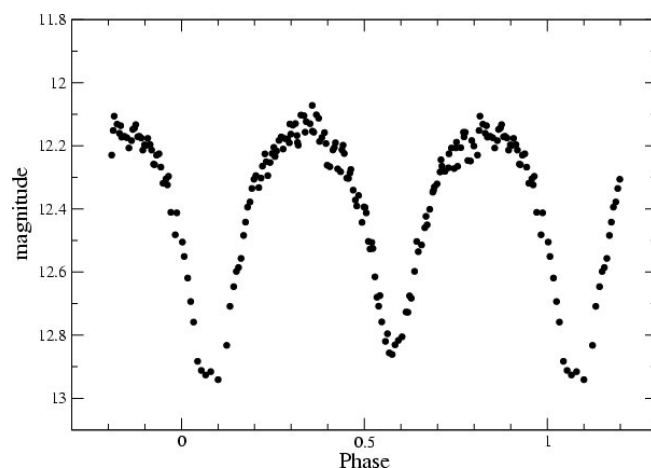
Figure 4.9: The lightcurve of a W UMa star with minima
almost equally deep, round and broad.[13]

---

[12]Figure   taken   from   http://www.boulder.swri.edu/~terrell/talks/aavso2001/
    betalyr.gif
[13]Figure taken from http://www.aanda.org/articles/aa/full/2003/43/aaINTEGRAL40/
    img43.gif

5 sdB - subdwarf B stars

Subdwarf B stars are subluminous stars with special pecularities presented further in the following sections. Hence, they can not be classified in the standard spectral classification schemes (e.g. the Yerkes classification, see section 2.3).
Most of the information was taken from Heber (2009).

5.1 Photometric characterization

Subdwarf B stars are core helium burning stars at the blue end of the horizontal branch, also called the extreme horizontal branch (EHB) (Lisker et al. 2005). There exists a difference between these two branches with regard to the luminosity. When the star is located in the HB the luminosity of the hydrogen burning shell is equal to or even exceeds the helium core luminosity, whereas in the EHB the luminosity of the hydrogen burning shell is negligibly small (Heber 1986).
From figure 2.3 it can be seen that the subdwarf B stars are located to the left and below the main sequence of hydrogen-burning stars. Their location indicates the range of temperature of the subdwarf B stars, too. Hence, their surface temperatures ranges from 25000 K to 40000 K and their surface gravities from $\log g = 5.0 \simeq 6.0$ (Maxted et al. 2001).
They appear both in the field, where they were found accidently by the search for faint blue stars like quasars, and in globular clusters, there just after a systematic search.
The Sloan Digital Sky Survey (SDSS) - a survey that helps to create 3-dimensional maps by photometrical and spectroscopical observations of more than a quarter of the sky - is a new rich source for hot subdwarf spectra, too. About 1100 hot subdwarfs were found in the SDSS spectral database (Geier et al. 2012). And the number of finding hot subdwarf stars increases. There are more hot subdwarf stars than any other type of faint blue objects to a magnitude limit of V = 18 mag.
Mostly found in binary systems escorted by at least one companion they live as well as single subdwarf stars. About half of the observed sdBs live in short period binaries with periods ranging from 0.07 days to more than 10 days (Geier et al. 2012). This is shown in figure 5.1, where the period distribution of 81 close sdB binaries is presented.

5.2 Evolution of sdB stars

Their evolution history is not yet completely understood because they do not fit into the textbook evolution schemes what makes these stars important to understand. But it is known that they must evolve directly into white dwarfs with core masses around $\sim 0.475 M_{\odot}$ (Heber & Hunger, 1984) because their H envelopes are too thin to maintain H burning. In comparison to their core masses their envelopes have very low masses of about $M_e \leq 0.02 M_{\odot}$.
Their weak metal lines let them appear to be of earlier spectral type than expected for normal dwarf stars. Due to helium diffusion, the He I lines in the spectra of subdwarf B stars are weak, too. In addition, the Balmer lines are well seen but abnormally broad for the colors of a main sequence B star.
In addition to everything mentioned above, subdwarf B stars help to understand galaxies because they are one of the main reasons for the UV upturn or excess in elliptical galaxies and bulges. Their discovery was suprising because it was known that elliptical galaxies
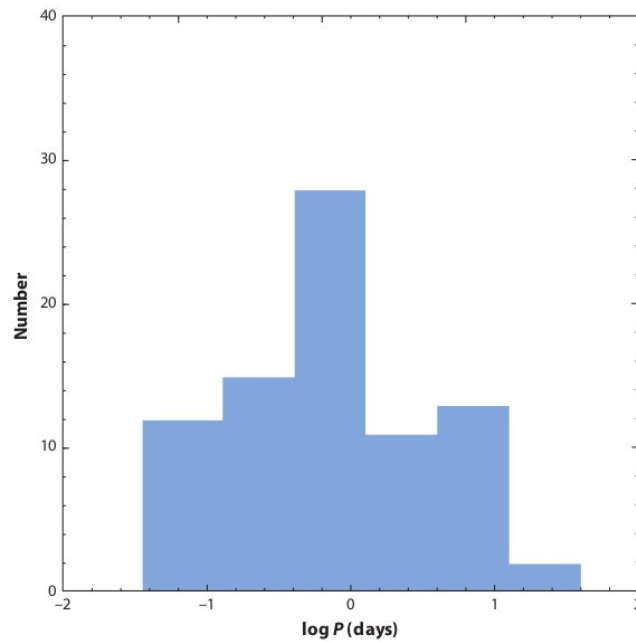
Figure 5.1: Period distribution of 81 subdwarf B stars. Most of the periods lie under one day, the average is at 0.61 days. This diagram is taken from Heber (2009).

contain mainly red old stars. Additionally, because of the long lifetime on the EHB at high temperatures in the Hertzsprung Russell diagram (compare to figure 2.3), they help to determine the age of elliptical galaxies (Brown et al. 1997, 2000).

Arguably, the most important role that close binary sdB stars may play in astrophysics, is that they qualify as SN Ia progenitors Maxted et al. (2000) if:

- the companion is a C/O white dwarf

- the total mass is close to the Chandrasekhar mass

- the merging time of the binary is shorter than the age of the Universe.

Some systems have been already found which will merge within a Hubble time (for more see Heber et al. 2003 or Geier et al. 2010).

5.3 Formation

The nature of subdwarf B stars can be summarized now straightforwardly in a few words: they are core-helium-burning stars with a mass distribution peaked around $\sim 0.47 M_\odot$ and a very thin hydrogen-rich envelope ($M_{env} < 0.01 M_\odot$). In addition, their high temperatures (25000-40000 K) locate them to the extreme horizontal branch (EHB).

But, in contrast to the characterizations, the progress in the understanding of evolution and formation of such a system is small.

In the paper of Heber et al. (1984) a large number of hypotheses of the evolution of subdwarf B stars was presented like the post horizontal branch evolution or the post red giant branch evolution of low mass stars. Sweigart et al. (1974) thought of helium core flash mixing and

Mengel et al. (1976) talked about a close binary evolution. But all these possible solutions were not good enough since there was no agreement with the observations or the proposed time scale was too short or, at that time, the rate of the events was not high enough. Hence, Heber et al. proposed in the same paper a simple alternative: to get well defined stellar parameters, like the effective temperature or the surface gravity by observations.

The proposition of Mengel et al. (1976) comes closest to the today's model of the formation of subdwarf B stars: they might be formed in close binary systems if the Roche lobe overflow occurs during the core helium flash.

Until now, approximately 40 years later, the problem lies still in the understanding of the formation and evolutionary status of these stars. The presently favoured scheme considers three formation channels,which were first presented and examined further by Han et al. (2002; 2003):

1. the Common-Envelope (CE) channel

2. the stable Roche Lobe OverFlow (RLOF) channel

3. the double helium White Dwarfs (WDs) merger channel.

These possible scenarios are discussed in more detail in the following and depend on the mass ratios in close binaries. Is the mass ratio $q \leq 1.2 - 1.5$ the mass transfer is stable and they can form the RLOF channel. If the mass ratio $a \geq 1.2 - 1.5$ the binary will form a common envolope and thus forming in a CE channel due to the unstable mass transfer.

5.3.1 The Common-Envelope (CE) channel

In this channel the subdwarf B stars are formed in short-period binaries with typical orbit periods between 0.1 to 10 days. This is a consequence of the dynamical mass transfer where the progenitor giant star starts to fill its Roche lobe when it is close to the tip of the first giant branch (FGB).

At this stage the radius of the mass-losing star increases faster than its Roche-lobe radius. This leads to a mass transfer on a dynamical time-scale and the formation of a common envelope, that is the giants envelope swallowing both, its degenerate core and the companion.

This mechanism was told to be the main mechanism of the CE.

When the star is close to the tip of the FGB at the beginning of the mass transfer the core is close to experience the helium flash whereas the remnant core still ignites helium and therefore becomes a helium-core-burning sdB star by ejecting the common envelope with the following possible companions:

- White dwarf if the sdB is the former secondary

- low-mass main sequence stars or brown dwarfs if the sdB is the former primary.

It is assumed that the common envelope is ejected when the change in orbital energy exceeds the binding energy of the envelope.

5.3.2 The stable Roche Lobe OverFlow (RLOF) channel

The stable Roche lobe overflow is based on the assumption that all transferred mass is transferred from the giant to the main sequence star in a stable way. No CE is formed and the separation of the components increases. The corresponding periods are of about 400 to approximately 1500 days. In comparison to the CE channel the sdB stars of this channel are predicted to have rather thicker hydrogen-rich envelopes.

This channel is based on stable mass transfer of a close binary system where the low-mass giant fills its Roche lobe on the FGB. There, it loses most of its envelope as a result of RLOF. The mass transfer stops when the hydrogen-rich envelope is sufficiently reduced and the radius of the star begins to shrink. If the mass of the degenerate core is still large enough it will experience the helium flash. For this scenario two subchannels are proposed - the first and the second stable RLOF. While the first stable RLOF occurs near the tip of the first giant branch, the second one occurs near the tip of the asymptotic giant branch. But in their simulations they found that sdBs formed in the second stable RLOF do not exist because the white dwarf companions are not massive enough. For more explications see the paper of Han et al. (2003).

Han, Podsiadlowski and Tout (2002) discussed that RLOF is more likely stable than believed before, as shown by the calculations mentioned there. They assumed a completely non-conservative mass transfer and that with all mass the system loses, all orbital angular momentum of the accreting component is lost. This process would support the observations of subdwarf B stars found on wide orbits (see Green, Liebert & Saffe 2001).

5.3.3 The double helium White Dwarf merger channel

Even a single sdB star can be formed from a close binary system via the merger of two helium white dwarfs, if their separations are so small that the binary merges within a Hubble time due to loss of angular momentum and energy by emission of gravitational waves. Thus, this double helium White Dwarf merger channel forms a single sdB star with a thin hydrogen-rich envelope and a wide mass distribution (0.4 to $0.65 M_\odot$). As the title indicates the channel assumes two helium white dwarfs in a close binary system. They are driven together and will merge. The final product is thus a single subdwarf B star if the merged object ignites helium.

5.4 HW Virginis systems

The HW Virginis systems are named after the first binary system discovered by Menzies & Marang (1986). They found that the faint blue star PG 1241-084 is a subdwarf B star with a short orbital period of 0.116719 days. The companion turned out to be a late M dwarf. The binary was then catalogued as HW Vir.

In general most of the known HW Virginis-like systems are binaries containing a subdwarf B star as primary and a late M dwarf as companion. The companion can only be seen by the large reflection effect caused by high temperature differences between primary and secondary which leads to a systematic contamination of the sdB spectrum by reflected light depending on the phase. In addition, the companion mass is small - about 0.1 to 0.2 $M_\odot$ which means that these stars are close to the nuclear-burning limit of $\simeq 0.08 M_\odot$ (i.e. the mass limit to a brown dwarf). Besides, they live in orbits of short periods of 0.1 days to 0.26 days.

Twelve known HW Virginis systems have been discovered during approximately 25 years, for example HS 0705+6700 (Drechsel et al. 2001) or NY Virginis (Kilkenny et al. 1998). For

HW Virginis two objects were found to orbit the binary at periods of 12.7 years and 55 ± 15 years and masses of $M_3 \sin i \simeq 14 M_{\text{Jup}}$ and $M_4 \sin i = 30 - 120 M_{\text{Jup}}$, respectively, making it a quadrupole system. Beuermann et al. (2012) presented a stable model after about 30 years of observations for this quadrupole system.

Pulsations of sdB stars in such binary systems can be found, too, like it was the case for NY Vir (Kilkenny et al. 1998).

The binary HS 2333+3927 shows similarity to all HW Virginis systems discovered yet. However, it is a non-eclipsing binary with light variations only due to reflection effect and ellipsoidal variability (Heber et al. 2004). More cases were found already (Schaffenroth 2010). In the paper of Geier et al. (2011), a HW Virginis system with a brown dwarf as companion and a short period of about 0.096 days has been presented.

This group of binaries has a high value for the research: it opens up the possibility to derive the mass of the sdB as well as the mass and nature of the companion by a combination of spectra and lightcurve analysis which helps to understand more and more what effects companions can have on the evolution in a binary and how a second and/or third body may influence the common envelope or even still exist after a CE ejection.

5.5 The MUCHFUSS project - Massive Unseen Companions to Hot Faint Underluminous Stars from SDSS

The MUCHFUSS project aims to find massive compact companions to hot subdwarfs, like white dwarfs with masses of $M > 1.0 M_\odot$, neutron stars or black holes. But this project can be used as well to find systems where planets, brown or white dwarfs companions caused the ejection of the common envelope (Geier et al. 2012).

The existence of such systems with subdwarf B stars plus neutron stars or black holes (sdB + NS/BH) is predicted by the binary evolution theory (Podsiadlowski et al. 2002). Hence, Geier et al. (2011b) concluded that "there must exist a population of non-interacting binaries with massive compact companions in our Galaxy" with low and high orbital inclinations. The fraction of these systems is predicted to be about 1% to 2% of the close subdwarf B binaries (Geier et al. 2010).

Motivated by these predictions Geier et al. (2010a,b) analyzed high resolution spectra of single-lined subdwarf B binaries with the aim to determine surface gravities and projected rotational velocities and the results are just consistent with companions as massive white dwarfs, neutron stars or black holes.

If the spectra are single-lined, the mass function and the minimum mass can be derived only. If the minimum mass exceeds $0.45 M_\odot$, too, the spectral features of main sequence stars become visible and the spectra are not anymore single but double lined. Therefore, having a single-lined spectrum and a derived minimum mass larger than $0.45 M_\odot$ it can be concluded that the companion has to be a compact object. If the mass is even larger than $1.0 \ M_\odot$ or $1.4 M_\odot$ the Chandrasekhar limit is reached an the companion must be a white dwarf, black hole or neutron star without any doubt. When the lightcurve is analyzed one can use the variations in the lightcurve to decide whether the companion is a substellar or a compact object because these variations are caused by the irradiated surfaces of the cool companion, also known as reflection effect. If the reflection effect is presented, the companion is most likely a main sequence star or a brown dwarf. If there is no reflection effect, an ellipsoidal variation with a period of half the orbital period would indicate that the companion is a

compact object.

The selection criteria of the MUCHFUSS project are tailored to single out radial velocities variations on time scales of half a day or less to indicate the presence of short period systems of relatively low RV amplitudes or longer-period binaries with high RV amplitudes.That means that subdwarf B stars with radial velocities $v_{\text{rad}} < \pm 100 kms^{-1}$ are excluded to filter out binaries with normal disc kinematics (Geier et al. 2011, 2012).

These selection criteria were already useful to find such close binary systems like the HW Virginis-like system that will be presented later in detail.

6 Analysis of SDSS 192059+372220.0 - a new HW Vir system discovered by MUCHFUSS

The MUCHFUSS collaboration has recently discovered a new HW Vir candidate, SDSS 192059+372220.0. In this thesis an analysis of time-series visual spectroscopy and photometry obtained at large telescopes will be presented. The analysis of the spectra that will be described in section 6.1 is complemented by the lightcurve analysis in section 6.2, and will allow us to derive the fundamental parameters of both companions of the system.

6.1 Spectral analysis

For the spectral analysis a spectrum is needed. One of the 54 spectra of the HW Virginis system SDSS 192059+372220.0 got from TWIN is plotted in figure 6.1, displaying exemplary the spectra range from 4000 to 5000 Å.
The spectrum of the sdB SDSS 1920 was observed and measured in the nights of the 13. August 2007 (four spectra from the SDSS database), 26., 27., 29., 30. May 2012 (39 spectra got from the TWIN spectrograph in Calar Alto) and 10., 11., 12. July 2012 (11 spectra got from the ISIS spectrograph at the William Herschel telescope in La Palma). The radial
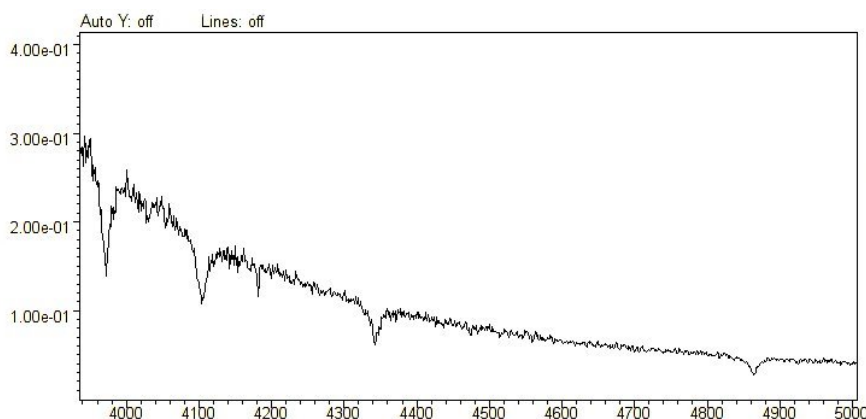
Figure 6.1: Spectrum of the SDSS 192059+372220.0. On the x-axis the used wavelength range in Å is given, on the y-axis the flux in arbitrary units.

velocities are derived from the Balmer lines and helium lines of the spectrum.

6.1.1 Barycentric corrections

All measurements are obtained at Earth-bound observatories and therefore have to be corrected for the motion and rotation of the Earth. A heliocentric reference system is often used. Because it is more precise, we choose the solar system barycentre, which lies inside the sun, for reference. Hence, all times of observations have to be corrected because of the finite speed of light. This so called barycentric correction can be as large as 8 minutes. In addition all spectra have to be corrected for the Doppler shift introduced by the motion of the Earth around the solar system barycentre and the Earth rotation.

6.1.2 SPAS - Spectrum Plotting and Analysis Suite

Using SPAS - the Spectrum Plotting and Analysis Suite - the spectrum of a star is spectroscopically analysed for effective temperature, surface gravity and helium abundance.
SPAS was developed by Heiko Hirsch to improve the user-friendless of the spectral analysis program developed by Ralf Napiwotzki - FITSB2.
SPAS is an user interface to fit parameters like for example the radial velocity to an observed spectrum to get the best fit parameters. It fits a model to a number of selected ranges. An example is seen in figure 6.2. Fitting a Gauss+Lorentz function to the observed spectrum
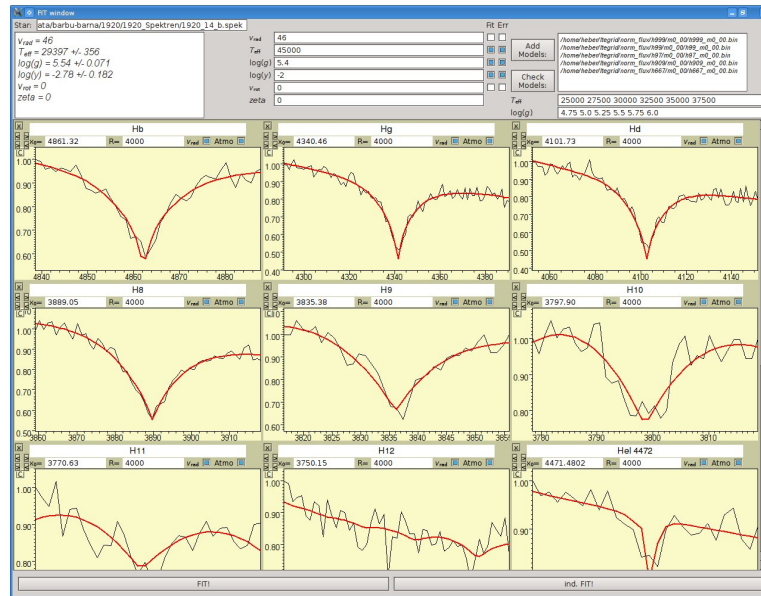
Figure 6.2: User interface of SPAS displaying the best fits to the hydrogen and helium lines of the sdB SDSS 192059+372220.0. Using Gauss+Lorentz functions the radial velocity of this observed spectrum is measured.

the radial velocity of the star can be measured. $v_{\rm rad}$ is then computed by using the Doppler formula :

$$\frac{\lambda - \lambda_0}{\lambda_0} = \frac{v_{\rm rad}}{c}$$

where $v_{\rm rad}$ is the radial velocity, λ_0 is the laboratory wavelength of the user selected spectral line and c the speed of light (Hirsch 2009). Every line is fitted separately and the mean radial velocity is taken from all fitted radial velocities.

6.1.3 Atmospheric parameters and the radial velocity curve

The observed spectra of SDSS 192059+372220.0 (short: SDSS 1920), reduced and normalized beforehand, were splitted in different spectral ranges. As typical for a subdwarf B (sdB), the hydrogen Balmer series is prominent beginning with H_β up to H_{12}. Only three helium lines have been found: He 4472, He 4026 and He 4922.
As can be seen in figure 6.3 the helium lines are really weak compared to the hydrogen lines of the same spectrum, in accordance to the classification of subdwarf B stars (chapter 5),
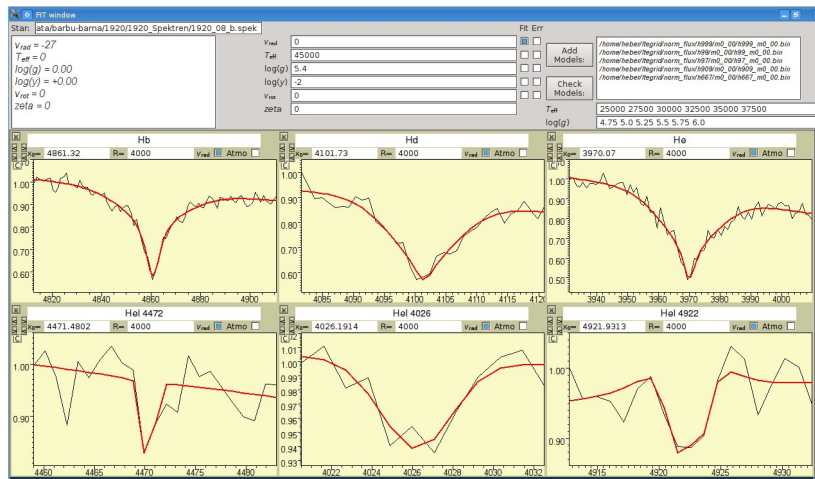
Figure 6.3: Hydrogen and helium lines comparatively. The hydrogen lines show a deep Δ flux of 0.4 to 0.5 dex whereas the helium lines show just a Δ flux of maximal 0.1 dex.

confirming that SDSS 1920 is indeed a sdB star.

SPAS was needed mostly to prepare the analysis of the radial velocity curve and to find both, the radial velocity and the atmospheric parameters like the effective temperature T_{eff}, the surface gravity $\log g$ and the helium abundance $\log y$, where $y = \frac{\text{Helium}}{\text{Hydrogen}}$ by number. Both seemed to vary with phase.

Atmospheric parameters

Due to the reflection effect the emitted spectra changes with the phase. The contribution of the companion to the continuum of the spectrum varies and, therefore, the derived atmospheric parameters of the primary seem to vary as well. In figure 6.4 and 6.5 we show these changes of effective temperature and surface gravity as a function of phase (see also table 6.1). At
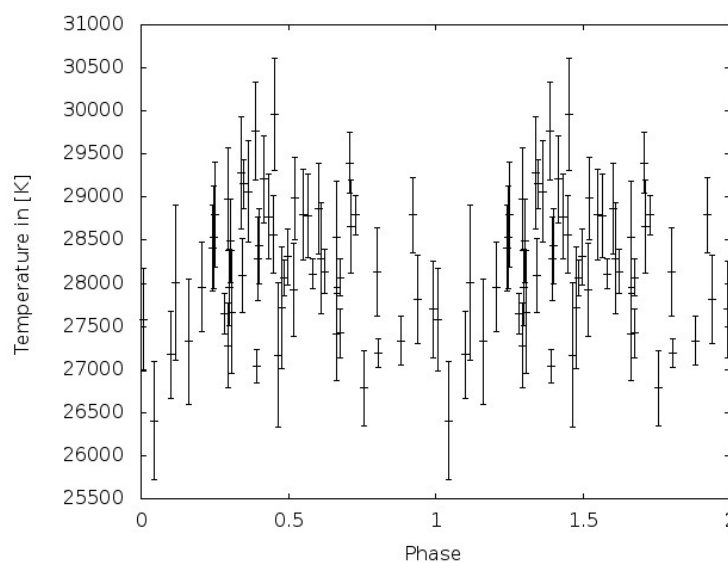
Figure 6.4: Change of the derived effective temperature with phase.
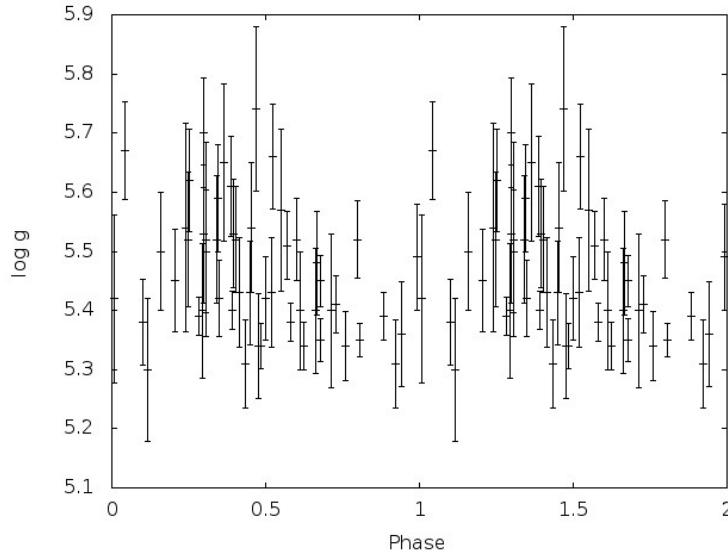
Figure 6.5: Change of the derived surface gravity with phase.

phase zero, the companion is in front of the primary (lower conjunction), i.e. the influence of the companion on the spectra is minimal. The same holds for the derived temperature and surface gravity of the sdB star. The temperature and the surface gravity seem to increase with the irradiance of the companion. Both, the derived temperature and surface gravity reach their highest at upper conjunction (phase 0.5). Beyond that the phase the derived effective temperature decreases.

A similar trend is expected for the surface gravity. Unfortunately, the scatter is too high to conclude whether the derived surface gravity varies with the phase. Since the companion is contributing to the light at every time, the derived temperature and surface gravity are never the "real" parameters. Consequently, the best estimate for effective temperature and surface gravity of the sdB star are the ones derived for phase zero where the contaminating light is minimal. Hence, we adopt the effective temperature and the surface gravity to $T_{\text{eff}} = 27600 \pm 600$ K and $\log g = 5.40 \pm 0.10$.

Figure 6.6 displays the position of SDSS 1920 in the $(T_{\text{eff}}, \log g)$-diagram. This binary system is located at the HW Vir system cluster (except three hotter ones) near the effective temperature of $T_{\text{eff}} = 28000$ K and a surface gravity of $\log g = 5.40$. They are a subgroup of the sdB stars, which are distributed widely in the $(T_{\text{eff}}, \log g)$-diagram.

Radial velocity curve

The derived radial velocity curve is shown in figure 6.7. The change of the radial velocity with the phase is well matched by a sine function.

The period was determined to 0.168830 days, the semiamplitude to $K_1 = 57.20 \pm 2.44$ kms^{-1} and the system velocity to $\gamma = 17.9 \pm 1.78$ kms^{-1}. For such a short period the system has to be formed in a common envelope phase (see chapter 5).

Due to the information derived from the radial velocity curve we can determine the mass function $f(M_1, M_2) = 0.003285592 M_{\odot}$. Assuming that the sdB star has the canonical mass of $0.47 M_{\odot}$ we derive $M_2 \sin i = 0.102 M_{\odot}$ which is close to the low mass limit of main sequence stars ($M = 0.08 M_{\odot}$). Bescause the system is eclipsing, the mass of the companion is only slightly higher (see table 6.2).

Phase	radial velocity [km s^{-1}]	temperature [K]	surface gravity $\log g$	helium abundance $\log y$	source
0.0075	+ 40±11	27578±602	5.42±0.142	-2.44±0.251	SDSS
0.0438	+ 28±10	26407±686	5.67±0.082	-2.86±0.164	TWIN
0.1027	+ 57±12	27172±506	5.38±0.073	-2.62±0.360	SDSS
0.1157	- 41±13	28429±754	5.30±0.121	-2.38±0.240	TWIN
0.1605	- 11±08	27324±725	5.50±0.099	-2.78±0.099	TWIN
0.2053	- 31±13	27959±524	5.45±0.087	-2.97±0.182	TWIN
0.2422	- 47±10	28407±496	5.54±0.177	-2.80±0.190	TWIN
0.2471	- 47±12	28533±594	5.52±0.114	-2.69±0.294	TWIN
0.2522	+ 23±09	28796±610	5.62±0.087	-2.84±0.105	TWIN
0.2832	+ 04±06	27645±233	5.39±0.033	-2.39±0.096	ISIS
0.2936	- 49±08	27280±494	5.40±0.114	-2.78±0.178	TWIN
0.2970	- 49±12	28602±817	5.70±0.093	-2.65±0.125	TWIN
0.2986	- 38±08	27954±442	5.53±0.117	-2.71±0.293	TWIN
0.3047	- 24±10	28490±485	5.50±0.103	-2.32±0.170	TWIN
0.3066	+ 52±11	27468±938	5.52±0.205	-2.54±0.190	SDSS
0.3418	- 36±13	29280±649	5.52±0.107	-2.79±0.315	TWIN
0.3451	- 21±13	28093±434	5.59±0.091	-2.47±0.146	TWIN
0.3500	- 39±09	29155±284	5.42±0.064	-2.71±0.306	TWIN
0.3647	- 44±13	29067±594	5.65±0.133	-2.67±0.173	TWIN
0.3878	- 44±10	29771±569	5.61±0.085	-2.74±0.273	TWIN
0.3928	- 31±09	27036±194	5.40±0.032	-2.40±0.155	ISIS
0.3966	- 08±10	28288±487	5.53±0.091	-2.42±0.135	TWIN
0.4015	- 36±10	28433±436	5.52±0.090	-2.56±0.141	TWIN
0.4159	- 14±13	29206±504	5.43±0.093	-2.33±0.191	TWIN
0.4327	- 56±10	28585±666	5.31±0.074	-2.68±0.325	TWIN
0.4480	+ 01±12	28567±445	5.43±0.088	-2.20±0.164	TWIN
0.4529	+ 06±13	28845±853	5.54±0.110	-2.13±0.199	TWIN
0.4674	- 27±11	27167±835	5.74±0.139	-2.51±0.205	TWIN
0.4775	- 18±08	27717±707	5.34±0.088	-2.82±0.368	TWIN
0.4863	- 49±10	28064±213	5.34±0.039	-2.37±0.096	ISIS
0.4996	+ 08±08	28306±320	5.42±0.070	-2.60±0.150	TWIN
0.5189	00±12	27927±539	5.43±0.093	-2.22±0.156	TWIN
0.5223	+ 03±12	28985±484	5.66±0.088	-2.70±0.277	TWIN
0.5510	+ 32±10	28796±530	5.57±0.137	-2.76±0.318	TWIN
0.5681	+ 29±08	28781±486	5.51±0.058	-2.07±0.283	TWIN
0.5815	- 42±06	28111±168	5.38±0.032	-2.43±0.082	ISIS
0.6025	+ 32±10	28870±528	5.52±0.069	-2.91±0.183	TWIN
0.6130	+ 37±13	28290±649	5.40±0.100	-2.50±0.239	TWIN
0.6225	- 17±08	28134±257	5.34±0.041	-2.21±0.105	ISIS
0.6626	+ 58±11	27414±536	5.40±0.106	-2.61±0.217	TWIN
0.6650	+ 42±10	28531±649	5.48±0.087	-2.95±0.398	TWIN

0.6773	00±06	27420±282	5.45±0.043	-2.45±0.121	ISIS
0.6780	- 20±12	28067±217	5.35±0.037	-2.41±0.117	ISIS
0.7099	+ 50±07	30394±648	5.83±0.249	-2.83±0.427	TWIN
0.7139	+ 63±13	28662±543	5.40±0.130	-2.52±0.303	TWIN
0.7295	+ 28±09	28794±228	5.41±0.049	-2.26±0.076	ISIS
0.7589	+ 57±13	26785±435	5.34±0.059	-3.04±0.494	TWIN
0.7996	+ 91±10	28135±509	5.52±0.066	-2.32±0.173	TWIN
0.8054	+ 55±08	27187±166	5.35±0.029	-2.34±0.095	ISIS
0.8839	+ 70±08	27333±286	5.39±0.041	-2.47±0.102	ISIS
0.9228	- 01±08	28508±859	5.27±0.110	-2.30±0.114	SDSS
0.9408	+ 58±13	27813±514	5.36±0.088	-2.41±0.120	TWIN
0.9923	+ 50±13	27696±556	5.49±0.089	-2.57±0.245	TWIN
used values		27600 ± 600	5.40 ± 0.10	-2.50 ± 0.250	

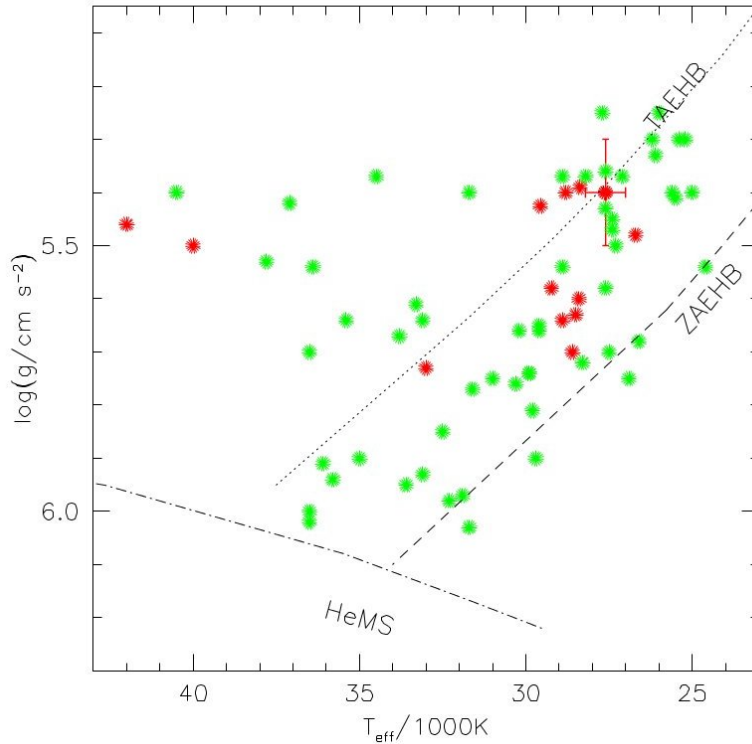Table 6.1: Change of the derived atmospheric parameters with phase.

Figure 6.6: Position of SDSS 192059+372220.0 (red) in the $(T_{\mathrm{eff}}, \log g)$-diagram, marked by an error cross. A sample of binary sdB stars (green) compiled by Heber (unpublished) is shown for comparison. Note the clustering of HW Vir star near $T_{\mathrm{eff}} = 28000$ K, $\log g = 5.5$ (Heber, priv comm.)
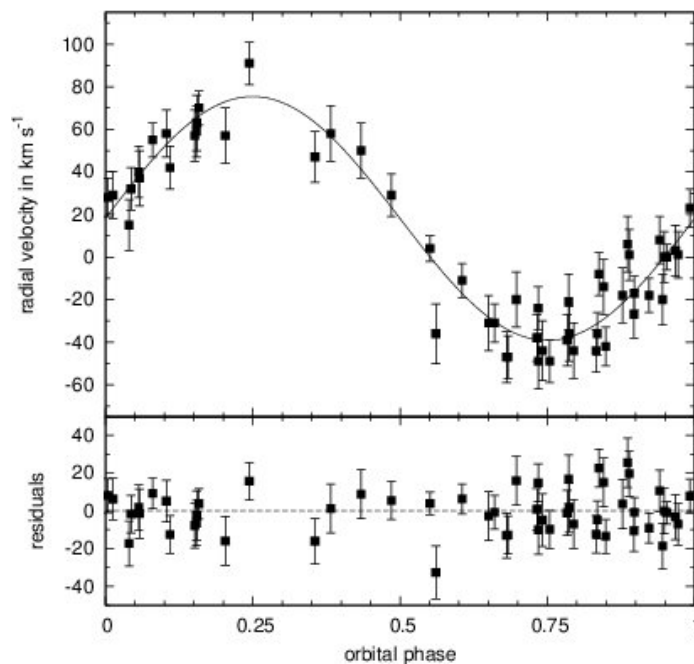
Figure 6.7: Radial velocity of SDSS 192059+372220.0. The best fit by a sinus function is shown by the black line. In the lower panel the residuals are displayed.

6.2 Photometric analysis

The form of the eclipses are dependent on the radii of both stars dependent on their separation, the inclination, the form of the stars and the mass and luminosity ratio. Therefore, a lightcurve analysis suits best to derive stellar parameters. With a combined analysis of spectroscopy and photometry, the absolute parameters like mass and radius can be determined.

To derive these stellar parameters a physical model is needed to calculate synthetic lightcurves and compare them to the observed ones. If the synthetic lightcurve fits best to the observations its parameters are regarded to be that of the system (Schaffenroth, 2010).

For this comparison, the Wilson-Devinney code (Wilson & Devinney 1971) is used to compute synthetic lightcurves. This model has 12+5n parameters, with n being the number of measured lightcurves, to calculate for every phase of the orbit the monochromatic flux of radiation emitted in the direction of the observer, while effects like gravity and limb darkening, reflection effect and rotational and tidal distortion are taken into account. The Roche Model (section 4.1.1) is the basis to determine the geometry of the stars.

Limb darkening

The limb darkening is due to the finite optical depth of the stellar atmosphere. An observer looks under a certain angle at the edge of the star in comparison to the center. Thus, the radiation received from the center comes from a hotter layer than those of the edge.

Gravity darkening

Due to stellar rotation and, thus, the centrifugal forces, the effective gravity at the equator is smaller than at the poles. Hence, in accordance with the theory of stellar atmospheres, the

flux does so, too.

Reflection effect

The reflection effect is an important effect visible in the lightcurve caused by a high temperature difference between primary and secondary. The companion is irradiated by the primary which leads to a heating of the companions' hemisphere. Thus, due to the higher temperatures, the emitted flux of the secondary is rising and therefore, the total emitted and increasing flux of the system is visible in the lightcurve, too.

In general, no reflection effect is visible when the two components of a binary system are equal. This effect is visible, even if no eclipses are measured.

The albedo $A_{1,2}$ gives the fraction of reradiated flux. Due to reprocessings in the atmosphere the albedo can rise to a value greater than one.

Determination of mass

When all these effects are taken into account in the lightcurve analysis, the radii (in units of the separation), the mass ratio and the inclination can be derived from the lightcurve. Hence, with the orbital parameters determined from the radial velocity curve the masses of both stars can in principle be derived:

$$M_1 = \frac{P}{2\pi G} \frac{K_j^3 \left(1 + q\right)^2}{q^3 \sin^3\left(i\right)} \text{ and } M_2 = qM_1. \tag{6.1}$$

However, in praxis, the mass ratio is only weakly constrained by the lightcurve.

To check the consistency of the spectroscopy and photometry a photometric surface gravity can be calculated from the derived parameters in the lightcurve:

$$g = \frac{GM}{R^2}. \tag{6.2}$$

6.2.1 MORO - MOdified ROche model

The explanations for MORO are taken from Schaffenroth (2010).

The program used to analyse the lightcurve of the HW Virginis system SDSS 1920 is called MORO - MOdified ROche model. This software was developed at the Dr. Karl Remeis Observatory in Bamberg. It is based on the Wilson-Devinney code 2 which does not restrict any system configurations and links luminosity and temperature of the second component by means of the Planck law. But in comparison to this code, MORO takes the radiative interaction between the components of hot and close binaries into account. However, this effect is negligable for SDSS 1920. For a closer look and a detailed description see the paper of Drechsel et al. (1995).

To derive all the stellar parameters from the lightcurve MORO uses the χ^2 minimization with the help of the Simplex-algorithm (Kallrath & Linnell, 1987). In this algorithm the Simplex, a m+1 set of start parameters, is defined by the user. Thus, for every parameter combination a synthetic lightcurve is calculated which is then compared to the observations. With the help of the residuals the mean square deviation is calculated by

$$\sigma_{fit}\left(x\right) = \sqrt{\frac{n}{n-m} \frac{1}{\sum_{\nu=1}^{n} w_\nu} \sum_{\nu=1}^{n} w_\nu d_\nu^2\left(x\right)}, \tag{6.3}$$

where $d_\nu = l_\nu^O - l_\nu^C$ is the difference between the calculated and the observed lightcurve, and w_ν the weight factor. The point of the Simplex with the worst σ_{fit} is deleted and it will be searched for another point with fixed operations until the convergence criterion is reached. Since the worst point is rejected this algorithm is stable because in every case a minimum will be found, although it has not to be a global one.

The set of parameters is large and the paremeters depend mostly on each other, so several solutions and minima are found. This degeneracy is highest for the mass ratio. Thus it is fixed for every run. The problem is, that the mass ratio is generally not known, so solutions for a range of mass ratios with each fixed mass ratio are derived. For the best solution, hence, the σ_{fit} of every solution is compared under each other. Since the minima of σ_{fit} do not differ a lot, the possible solution has to be selected after verifying other derived parameters, like radius or possible masses for both, primary and companion. This solution has to be compared to the derived results from the spectroscopical analysis, too.

6.2.2 BUSCA lightcurves

Figure 6.8: BUSCA - Bonn University Simultaneous Camera (Schaffenroth 2010).

The lightcurves were measured with BUSCA, the Bonn University Simultaneous Camera, which observes simultaneously in four different bands, the UV, B, R and NIR channel. Thanks to BUSCA, the time of observation is shortened and no light is lost. Hence, it is an ideal instrument to measure lightcurves.

Most importantly, the lightcurves are recorded simultaneously in four different wavebands, reducing the influence of variable night sky conditions. BUSCA and the transmission curves of the different BUSCA channels are displayed in figure 6.8 and 6.9. The functionality of BUSCA is described in detail in Schaffenroth (2010).

In figure 6.10 the four lightcurves observed with BUSCA are displayed. Unfortunately, the scatter was too high and the comparison stars which are important to reduce the lightcurves were not blue enough. Therefore, the lightcurves from the UV and the NIR channel were not used for the photometric analysis.

The reflection effect is clearly visible in the lightcurves. Both eclipses, the primary and the secondary are visible.
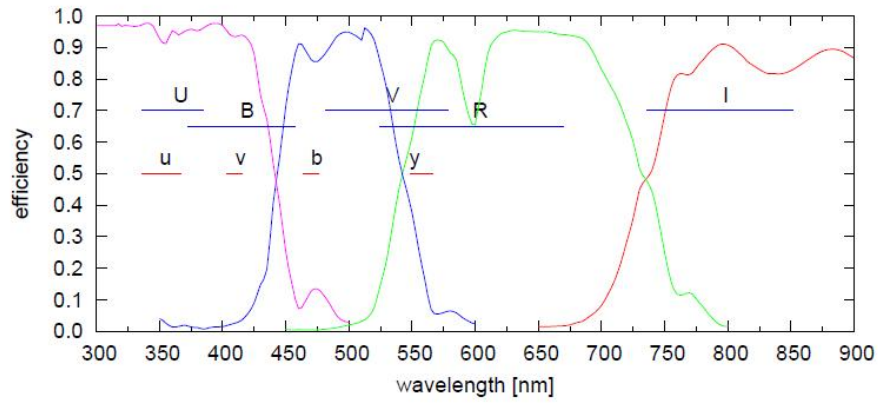
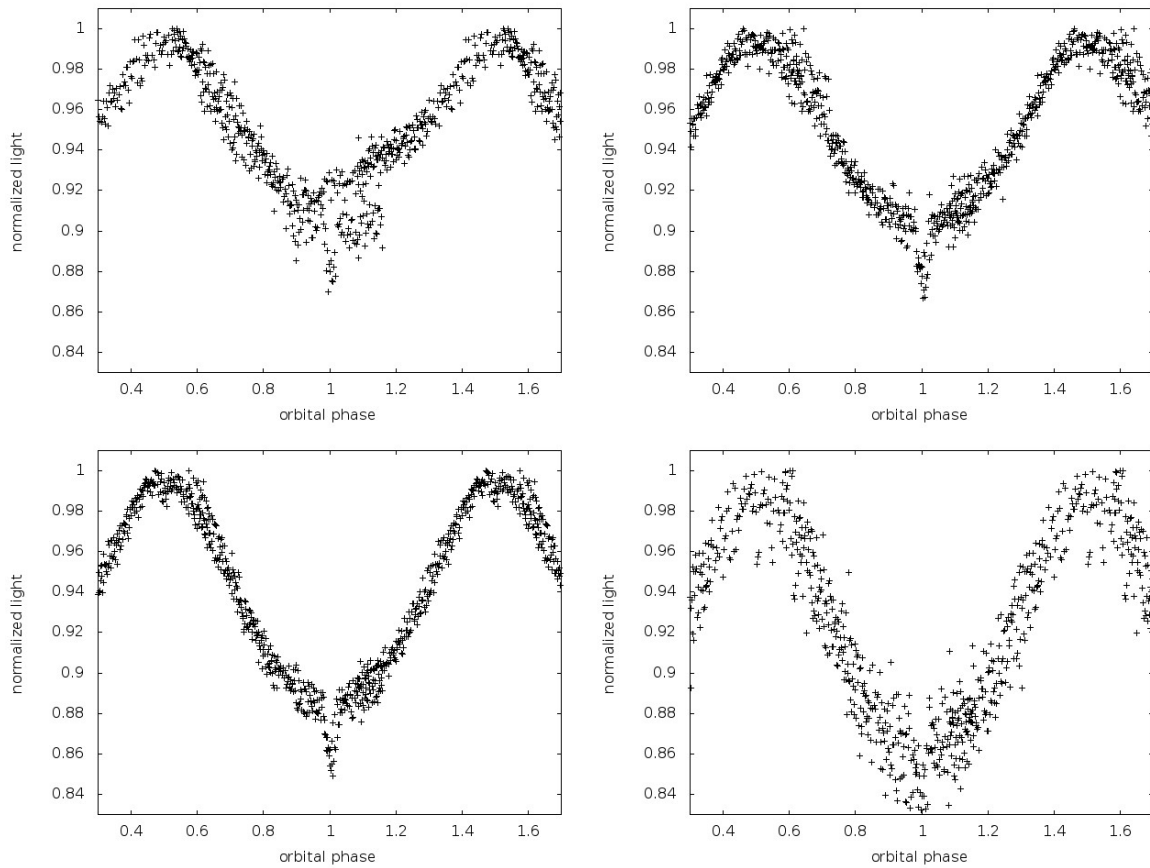Figure 6.9: Transmission curve of the different BUSCA channels (Schaffenroth 2010).

Figure 6.10: The four lightcurves of SDSS 192059+372220.0 observed with BUSCA.

Fixed parameters			Adjustable parameters			Roche radii		
$q\left(\frac{M_2}{M_1}\right)$		0.24	i	[°]	65.541	r_1 (pole)	[a]	0.272
$T_{\text{eff},1}$	[K]	28000	$T_{\text{eff},2}$	[K]	2544	r_1 (point)	[a]	0.278
g_1		1.0	A_1		0.770	r_1 (side)	[a]	0.275
g_2		0.32	A_2		0.570	r_1 (back)	[a]	0.277
$x_1(500)$		0.25	Ω_1		3.702			
$x_1(650)$		0.21	Ω_2		2.597	r_2 (pole)	[a]	0.194
δ_2		0.00	δ_1		0.055	r_2 (point)	[a]	0.197
l_3		0.00	$x_2(500)$		0.999	r_2 (side)	[a]	0.197
			$x_2(650)$		0.999	r_2 (back)	[a]	0.207

Table 6.2: Outline of the fixed and adjustable parameters for the canonical solution of the lightcurve analysis of SDSS 192059+372220.0

6.2.3 Results of the photometric analysis

On account of the high luminosity ratio and the companions' visibility caused only by the reflection effect and the eclipses, the Wilson-Devinney mode selected is not important. Consequently, the derived effective temperature of the secondary is not reliable because of the simplified assumption that the secondary radiates as a black body. Since the number of lightcurve parameters is high (12+5n = 22), the number of free parameters has to be reduced with the help of spectroscopy or theory.

The choise of parameters listed in table 6.2 is explained in the diploma thesis of Schaffenroth (2010).

The mass ratio, the temperature of the primary as well as $g_1, g_2, x_1(500), x_1(650)$ and $\delta_2 = 0.00$ were fixed. The companion is so cool, that no deformation of the companion due to radiation pressure is expected. For the primary, the remaining parameters are allowed to vary. The limb darkening coefficients (Claret & Bloemen 2011) were extrapolated and found to be $x_1(500) = 0.250$ and $x_1(600) = 0.210$. Due to the reflection effect, the limb darkening of the companion is not predictable. Therefore, x_2 was allowed to vary.

q	σ_{fit}
0.19	0.005543
0.20	0.005547
0.21	0.005532
0.22	0.005439
0.23	0.005512
0.24	0.005507
0.25	0.005438
0.26	0.005457
0.27	0.005481
0.28	0.005467

Table 6.3: Outline of the different derived σ_{fit} for each mass ratio.

Table 6.2 presents the solution for the canonical mass of the sdB primary of $M_{\text{sdB}} = 0.47 M_\odot$. The inclination i derived from this lightcurve analysis is a reliable value which is necessary to determine the possible masses for both stars of the binary, as well as the derived radii. The derived value for the albedo A_2 is larger than 1 as briefly explained in section 6.2. Besides, the effective temperature $T_{\text{eff},2}$ for the companion is not reliable as described above.

The solution for the canonical sdB mass is not the only one.

Due to the degeneracy of the mass ratio q (see 6.2.1), table 6.3 presents the different σ_{fit} for the possible mass ratios. They do not differ much. Therefore, there exist possibilities which fit to the lightcurve analysis, too. Hence, to find the possible best solutions the determined values derived from the photometric analysis have to be compared with theory for surface

gravity, radius and mass.

The mass ratios q = 0.19, q = 0.20 and q = 0.21 were excluded as possible solutions because the masses for the primary are too high. Those solutions would require the binary to be formed in the merger channel.

q = 0.23, q = 0.26 and q = 0.27 as mass ratios were excluded due to the high difference between the surface gravity derived spectroscopically ($\log g = 5.40 \pm 0.10$) and photometrically ($\log g = 5.26 \pm 0.02, \log g = 5.27 \pm 0.02$ and $\log g = 5.26 \pm 0.02$ respectively).

To determine a consistent solution the photometrical and spectroscopical surface gravity have to match. The solution for a mass ratio of q = 0.22 is a possible solution for the binary system because it maches well with the surface gravity derived from the spectroscopic analysis. Therefore this solution cannot be excluded although, the derived mass $M = 0.561 \pm 0.07 M_\odot$ is higher than predicted for a binary system formed in the CE channel. More analysis is needed to confirm or exclude this possibility.

Possible solutions for the binary which fits with all criteria are thus q = 0.22, q = 0.24 and q = 0.25.

Therefore, figure 6.11 displays the photometric surface gravity dependent on the mass of
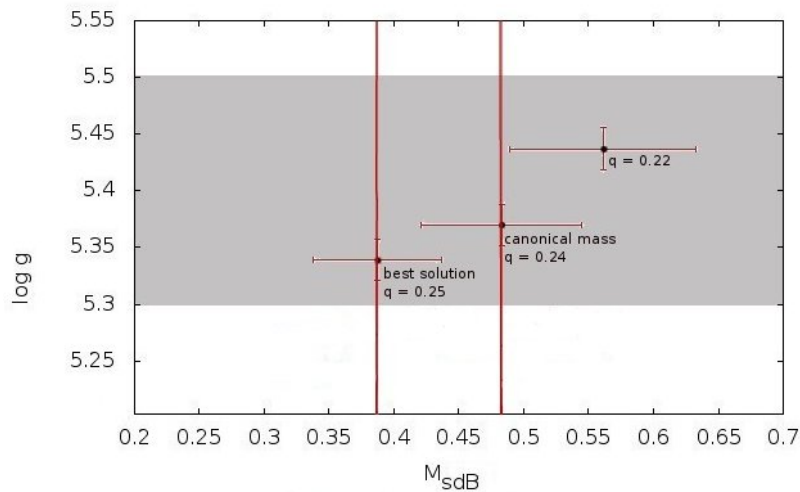

Figure 6.11: The photometric surface gravity dependent on the mass of the subdwarf B primary. The grey range displays the spectroscopic value with error range.

the subdwarf B primary in solar masses. The range shaded grey displays the spectroscopical solution for the surface gravity with the error range. Both solutions, the canonical and the best one, fit to the spectroscopical solution for the surface gravity taking the grey error range also into account.

In figure 6.13 the best lightcurves with the best fits are presented at the mass ratio of $q = 0.24$. As mention above, the reflection effect is clearly visible in the lightcurves. Both, the primary and the secondary eclipses are visible. However, the eclipses are not total.

Nevertheless, the theoretical line is not yet deep enough for the primary eclipse, showing that this solution is not yet the best one.

In figure 6.14 the equipotential surfaces of both stars are displayed. According to the photometric solution, the system is detached. Both stars lie well inside their Roche lobes. The primary is bigger than the secondary. Both stars are still spherical.
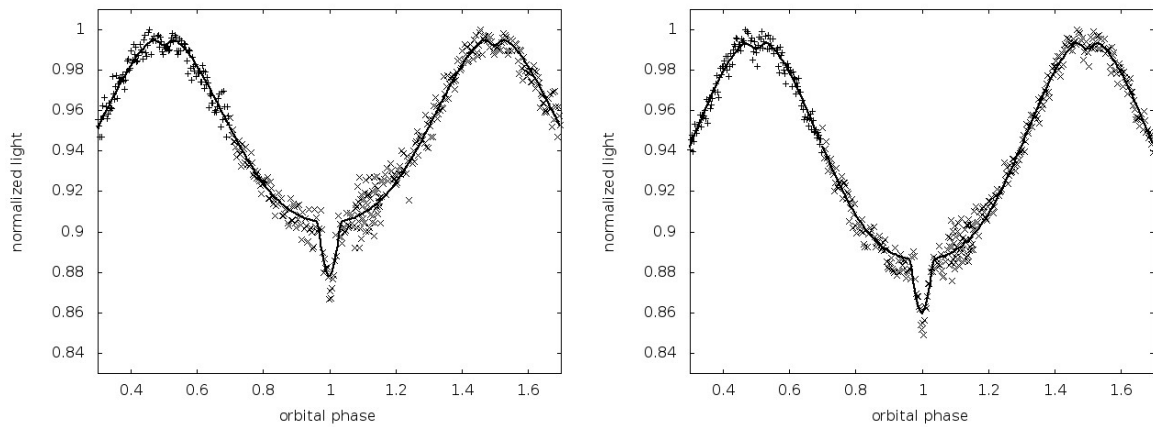
Figure 6.12: The V band lightcurve ($\lambda = 500$ nm) of SDSS 192059+372220.0 on the lefthand panel and the R band lightcurve ($\lambda = 650$ nm) on the righthand panel. The black lines present the best fit to the normalized lightcurves.
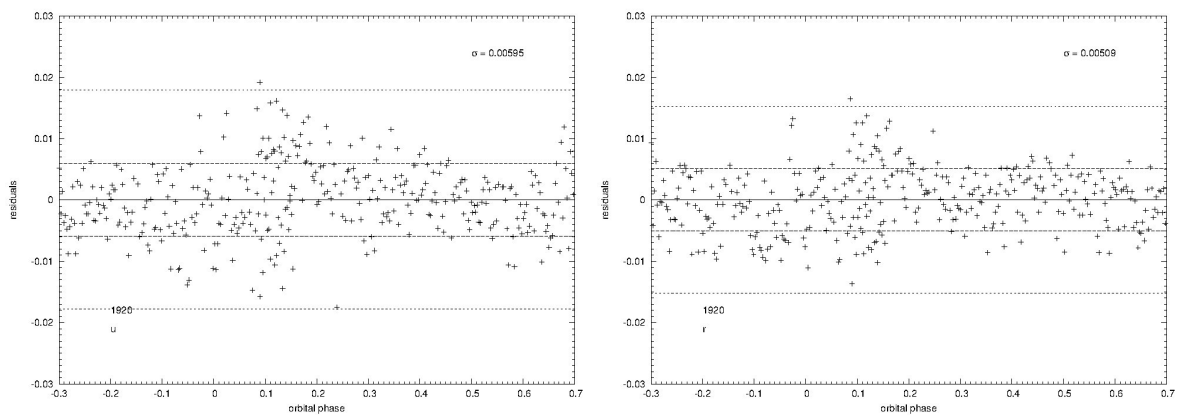

Figure 6.13: The residuals of SDSS 192059+372220.0 of the V band on the lefthand panel and of the R band on the righthand panel are shown.
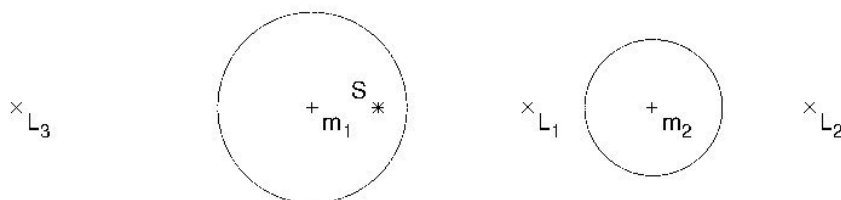

Figure 6.14: The equipotential surfaces and Langrangian points of the binary system SDSS 192059+372220.0.

6.3 Discussion

With q = 0.24 the mass ratio was fixed for the possible solution for the canonical mass of the primary. Thus, the radii of the stars, in units of the separation, are derived by means of the lightcurve analysis. Using the mass function derived from the radial velocity curve the absolute parameters and therefore, the nature of the companion can be determined. These absolute parameters are presented in table 6.4, as well as the parameters for the best σ_{fit} solution - q = 0.25 - and q = 0.22.

		"Best solution"	canonical mass solution
M_{sdB}	$[M_\odot]$	0.387 ± 0.049	0.483 ± 0.062
M_{comp}	$[M_\odot]$	0.096 ± 0.012	0.115 ± 0.014
a	$[R_\odot]$	1.010 ± 0.043	1.084 ± 0.046
R_{sdB}	$[R_\odot]$	0.220 ± 0.009	0.299 ± 0.013
R_{comp}	$[R_\odot]$	0.161 ± 0.006	0.216 ± 0.009
$\log g(1)$		5.33 ± 0.018	5.36 ± 0.018

Table 6.4: Absolute parameters of SDSS 192059+372220.0 - best solution and canonical mass solution comparatively, calculated with the help of the mass function and the lightcurves.

Both presented masses for the primary ($0.483 M_\odot$ and $0.387 M_\odot$) are in accordance with theoretical predictions. With its mass of $0.115 M_\odot$ ($0.096 M_\odot$) and its radius of $0.216 R_\odot$ ($0.161 R_\odot$) the companion has to be a M dwarf.

From the radial velocity curve the mass function is derived. As described in section 6.2 the canonical mass is assumed as mass for the primary. Not knowing if this assumption is correct, different mass ratios around the canonical mass are analysed in the photometric analysis and then compared to the derived spectroscopic values to find the best solutions. In this case, three mass ratios, q = 0.22, q = 0.24 and q = 0.25 are possibilities for a consistent photometric and spectroscopic analysis. Nevertheless, needing more spectra and lightcurves to confirm or exclude the other solutions, it is more reliable to base this analysis on theory with a mass ratio of q = 0.24. Therefore, SDSS 192059+372220.0 is a typical HW Virginis system containing a subdwarf B primary and a M dwarf secondary.

6.4 Summary

In this Bachelor thesis a spectroscopic and photometric analysis of a new HW Vir system, SDSS 192059+372220.0 is presented. The Observations were obtained from the DSAZ, Calar Alto and ING, La Palma.
Being a single-lined spectroscopic binary, the primary was identified to be a subdwarf B star. The reflection effect is here higher than in the "normal" Algol systems, what makes this system the thirteenth known existing systems of the group of HW Virginis, named after the prototype.
This binary system is visible under an inclination of $i = 65.541°$ and is therefore a partially eclipsing binary. The companion is seen all the time, even behind the primary. Therefore, the best values for the surface parameters are derivable with the smalles contamination of light - at phase zero. Hence, the effective temperature was determined to be $T_{\mathrm{eff}} = 27600 \pm 600$ K and the surface gravity was approximately determined to $\log g = 5.40 \pm 0.10$, all in accordance with the presented theory in this thesis and the photometric analysis with a value of $\log g = 5.36 \pm 0.02$.
SDSS 1920 has a separation of $a = 1.084 \pm 0.046\ R_{\odot}$ and the photometric analysis tells us the system to be detached, therefore an Algol binary.
Due to the short period of 0.168830 days this binary has to be formed in a common envelope phase.

Unfortunately, the period is not precise enough to determine the ephemerides. For the future high resolution spectra are needed to find out if the binary system has a synchronised rotation like our moon by making use of the Rossiter- McLaughlin effect. As well, with more high resoluted lightcurves from more nights a closer look at the period would be possible. The scatter of the observed lightcurves was high and the comparison stars to reduce the lightcurves were not blue enough, so a perfect solution for this system is not yet found. More lightcurves and more work on the lightcurve analysis will improve the photometric analysis and yield more accurate in particular the mass ratio. As well, knowing that the scatter of the spectra was too high to derive a visible dependance of the surface parameters on the phase, more spectra with smaller scatter would help to determine better these atmospheric parameters and therefore derive a more precise value for the mass function, too.

The further search for such binary systems could help us to keep on growing our understanding for the formation of subdwarf B stars in close binary systems. The question why nearly all HW Vir systems were found in the $(T_{\mathrm{eff}}, \log g)$ diagram nearly at the same effective temperature and surface gravity could be answered or if this is only a coincidence and the next found HW Vir stars will be located at a different position.
Besides, a long term observation of several years could give us information of third bodies via eclipse timing, influencing the binary system as it was the case of the prototype HW Vir (Beuermann et al. 2012). Hereby it would be interesting to know, if and how third bodies survive a common envelope or if they form after a common envelope ejection.

7 Appendix

Fixed parameters			Adjustable parameters			Roche radii		
$q\left(\frac{M_2}{M_1}\right)$		0.25	i	[°]	70.997	r_1 (pole)	[a]	0.216
$T_{\text{eff},1}$	[K]	28000	$T_{\text{eff},2}$	[K]	3690	r_1 (point)	[a]	0.219
g_1		1.0	A_1		0.28	r_1 (side)	[a]	0.218
g_2		0.32	A_2		1.95	r_1 (back)	[a]	0.219
$x_1(500)$		0.25	Ω_1		4.779			
$x_1(650)$		0.21	Ω_2		2.956	r_2 (pole)	[a]	0.156
δ_2		0.00	δ_1		0.0165	r_2 (point)	[a]	0.160
l_3		0.00	$x_2(500)$		0.389	r_2 (side)	[a]	0.158
			$x_2(650)$		0.389	r_2 (back)	[a]	0.162

Table 7.1: Outline of the fixed and adjustable parameters for the best σ_{fit} solution of the lightcurve analysis of SDSS 192059+372220.0 for the mass ratio q = 0.25.

Fixed parameters			Adjustable parameters			Roche radii		
$q\left(\frac{M_2}{M_1}\right)$		0.22	i	[°]	69.135	r_1 (pole)	[a]	0.208
$T_{\text{eff},1}$	[K]	28000	$T_{\text{eff},2}$	[K]	4946	r_1 (point)	[a]	0.209
g_1		1.0	A_1		0.060	r_1 (side)	[a]	0.209
g_2		0.32	A_2		1.180	r_1 (back)	[a]	0.209
$x_1(500)$		0.250	Ω_1		4.983			
$x_1(650)$		0.210	Ω_2		2.518	r_2 (pole)	[a]	0.191
δ_2		0.00	δ_1		0.008	r_2 (point)	[a]	0.208
l_3		0.004	$x_2(500)$		0.254	r_2 (side)	[a]	0.196
			$x_2(650)$		0.254	r_2 (back)	[a]	0.206

Table 7.2: Outline of the fixed and adjustable parameters for the best solution of the lightcurve analysis of SDSS 192059+372220.0 for the mass ratio q = 0.22.

8 Bibliography

Beuermann, K., Dreizler, S. Hessman, F.V. Deller, J.: 2012, A&A 543, A138

Brown, T.M., Ferguson, H.C., Davidsen and A.F., Dorman, B.: 1997, The Astrophysical Journal, 482:685

Brown, T.M., Bowers, C.W., Kimble, R.A. and Ferguson, H.C.: 2000, The Astrophysical Journal, 529:L89

Claret, A., Bloemen, S.: 2011, A&A, 529, A75

Carroll, B., Ostlie, D.: 2007, *An Introduction to Modern Astrophysics*, Pearson Education, second edition

Drechsel, H., Heber, U., Napiwotzki, R. et al. 2001, A&A 379, 893

Drechsel, H., Haas, S., Lorenz, R., Gayler, S.: 1995, Astron. Astrophys., 294, 723

Edelmann, H., Heber, U., Hagen, H.-J. et al. 2003, A&A 400, 939

Falter, S., Heber, U., Dreizler, S., et al.: 2003, A&A 401, 289

Geier, S., Heber, U., Kupfer, T., Napiwotzki, R.: 2010, A&A 515, A37

Geier, S., Heber, U., Podsiadlowski, Ph., et al.: 2010, A&A 519, A25

Geier, S., Schaffenroth, V., Drechsel, H. et al.: 2011, The Astrophysical Journal Letters, 731:L22

Geier, S., Maxted, P. F. L., Napiwotzki, R. et al.: 2011a, A&A 526, A39

Geier, S., Hirsch, H., Tillich, A. et al.: 2011b, A&A 530, A28

Geier, S., Schaffenroth, V., Hirsch, H. et al. Astron. Nachr. 333, No.5/6, 431

Han, Z., Podsiadlowski, P., Tout, C.A.: 2002 ASP Conferences Series 279

Han, Z.; Podsiadlowski, P.; Maxted, P. F. L., Marsh, T. R.: 2003, Monthly Notices of the Royal Astronomical Society, 314, 669

Han, Z.; Podsiadlowski, P.; Maxted, P. F. L.; Marsh, T. R. and Ivanova, N.: 2002, Monthly Notices of the Royal Astronomical Society, 336, 449

Heber, U., Junger, K., Jonas, G., Kudritzki, R.P.: 1984a, Astron. Astrophys. 130, 119

Heber, U.: 1986, Astron. Astrophys. 155, 33

Heber, U., Hunger, K.: 1984, ESO Messenger 29

Heber, U., Edelmann, H., Lisker, T., Napiwotzki, R.: 2003, A&A 411,L477

Heber, U., Drechsel, H., Østensen, R. et al.: 2004, A&A 420, 251

Heber, U.: 2009, Annu. Rev. Astron. Astrophys., 47, 211

Hilditch, R.W.: 2001, *An Introduction to Close Binary Stars*, Cambridge Unisersity Press

Hirsch, H.: 2009, Dissertation an der Friedrich-Alexander-Universität Erlangen-Nürnberg

Iben, I.: 1965, Astrophysical Journal, 141,993

Karttunen, H., Kröger, P., Oja, H. et al. 2007, *Fundamental Astronomy*, Springer Verlag, 5th edition

Kallrath, J., Linnell, A.P.: 1987, The Astrophysical Journal, 313:346

Kilkenny, D., O'donoghue, Koen, C. et al.: 1998, MNRAS, 296, 338

Lisker, T., Heber, U., Napiwotzki, R. et al. 2005, Astronomical Society of the Pacific, 303

Maxted, P. F. L., Marsh, T. R., North, R. C.: 2000, MNRAS, 317, L41

Maxted, P. F. L., Marsh, T. R., North, R. C.: 2001, ASP Conferences Series 226

Maxted, P. F. L., Heber, U., Marsh, T. R., North, R.C.:2001, MNRAS 326, 1391

Mengel,J.G., Norris J., Gross P.G.: 1976, The Astrophysical Journal, 204:488

Menzies, J.W., Marang, F., 1986, International Astronomical Union, 118, 305

Nagel, K.: 2012, Zulassungsarbeit an der Friedrich-Alexander-Universität Erlangen-Nürnberg

Østensen, R.H., Oreiro, R., Haili Hu et al. 2008, ASP Conferences Series 392

Podsiadlowski, Ph., Rappaport, S., Pfahl, E. D.:2002, The Astrophysical Journal, 565:1107

Qian, S.-B., Zhu, L.-Y., Zola, S. et al.: 2009, The Astrophysical Journal, 695:L163

Schaffenroth, V.: 2010, Diplomarbeit an der Friedrich-Alexander-Universität Erlangen-Nürnberg

Sweigart, A.V.: 1974, The Astrophysical Journal, 189:289

Schaffenroth, V., Geier, S., Drechsel, H. et al.: 2012, A&A, 553, A18

Wilson, R.E., Devinney, E.J.: 1971, The Astrophysical Journal, 166:605

9 Danksagung

10 Erklärung

Hiermit erkläre ich, Ingrid Barbu-Barna, dass ich die vorliegende Bachelorarbeit selbstständig verfasst habe und keine anderen als die angegebenen Hilfsmittel und Quellen verwendet habe.

Erlangen, den 14. August 2013   Ingrid Barbu-Barna